CORONAL MASS EJECTIONS AND PROBLEM THEY CAUSE ON EARTH

By

Debela Alemayehu Gashe

A THESIS SUBMITTED TO

GRADUATE PROGRAMS OF
ADDIS ABABA UNIVERSITY

IN PARTIAL FULFILLMENT FOR THE REQUIREMENTS
OF THE DEGREE

MASTER OF SCIENCE IN PHYSICS

(ASTRONOMY/ASTROPHYSICS)

ADDIS ABABA, ETHIOPIA

OCTOBER 2020

ADDIS ABABA UNIVERSITY

PROGRAM OF GRADUATE STUDIES

CORONAL MASS EJECTIONS AND PROBLEM THEY CAUSE ON EARTH

By

Debela Alemayehu Gashe

Department of Physics

Addis Ababa University

Approved by the Examining Board:

Dr. Remudin Reshid Advisor	_____ Signature
Dr. Teshome Senbeta Examiner	_____ Signature
Dr. Tilahun Tesfaye Examiner	_____ Signature

Date: October 2020

ADDIS ABABA UNIVERSITY

Date: **October 2020**

Author: **Debela Alemayehu Gashe**

Title: **Coronal Mass Ejections and Problem they Cause on Earth**

Department: **Department of Physics**

Degree: **M.Sc.** Convocation: **October** Year: **2020**

Permission is herewith granted to Addis Ababa University to circulate and to have copied for non-commercial purposes, at its discretion, the above title upon the request of individuals or institutions.

_____

Signature of Author

This Work is Dedicated

to My parents

Table of Contents

Table of Contents v

List of Figures vii

Acknowledgements x

Abbreviations xi

Physical Constants xiii

Symbols xiv

Abstract xv

1 Introduction 1

2 CMEs basic review and their impact on the earth 4

2.1 An overview of the sun and its active regions 4

2.1.1 The sun's interior 4

2.1.2 The sun's atmosphere 6

2.1.3 Heating of the chromosphere and corona. 10

2.1.4 Solar activity in the photosphere: sunspots. 11

2.1.5 Magnetism and solar cycle 12

2.1.6 Differential rotation of the sun 14

2.1.7 Solar activity above the photosphere: prominence and flare . 15

2.2 Coronal mass ejections (CMEs) 15

2.2.1 A brief history of CMEs 16

2.2.2 Observations of CMEs 17

2.2.3 Properties of CMEs 20

2.2.4 Theoretical CMEs models 24

2.3 CMEs-Geomagnetic storm impacts 26

2.3.1 Disruptions to electrical systems 27

2.3.2 Problems in communications and navigation systems 29
2.3.3 Satellite hardware damage 30
2.3.4 Problems in geologic exploration and hazard in pipelines . . . 31
2.4 CMEs and their impact: summary 31

3 Methods for analysis of geomagnetic storms and GICs during CMEs directed to the earth 32

3.1 CME-Geomagnetic storms 32
3.2 Phases and severity of geomagnetic storms 32
3.3 Disturbance storm time index (Dst-index) 33
3.4 Data sources for Dst-index and SSN 33
3.5 Analytical approach to fields and GICs 34
3.5.1 Magnetoquasistatic equations 35
3.5.2 Derivation of magnetic diffusion equation 36
3.5.3 Physical set up of certesian coordinate 36
3.5.4 Solutions of the magnetic diffusion equation 36
3.5.5 Ground current density and electric field 38
3.5.6 Earth's surface impedance 39

4 Results And Discussion 40

5 Conclusion 49

Bibliography 51

List of Figures

2.1 A basic overview of the parts of the sun (from SOHO images of the sun) 6

2.2 The solar corona at a time close to solar minimum (Image: Fred Espernak) 9

2.3 Photo of a sunspot on the solar surface:NASA/courtesy of nasaimages.org. 12

2.4 Sunspot cycle during the past century (Image: courtesy of NASA MSFC) 13

2.5 The sun rotates more quickly at its equator than it does near its poles. Because gas circles the sun faster at the equator, it drags the sun's north-south magnetic field lines into a more twisted configuration. The magnetic field lines linking pairs of sunspots, depicted here as dark blobs, trace out the directions of these stretched and distorted field lines [15] 14

2.6 Some spacecraft obsevatory in the heliosphere that studying the sun and the sun-earth environment [34] 19

2.7 A three-part CME with the core, cavity, and bright front marked (Credit: SOHO/ LASCO CME Catalog) 21

2.8 Flux cancellation model showing the erupting flux rope at two different heights. a) Close to the sun flux rope is in equilibrium and b) at a larger distance it is unstable against gravitational pull of the sun. Here, a current sheet is formed beneath the flux rope [43]. 26

2.9 Magnetic field lines during the eruption process based on the magnetic breakout model. The flux rope system rises and reconnects with the overlying magnetic field lines. A current sheet is built behind an isolated flux rope and magnetic reconnection then leads to the eruption of the flux rope [45] 27

2.10 Earth's magnetosphere [48] 28

2.11 All of the above space based and ground based technologies, and geospace environment are disrupted durng severe geomagnetic storm [31]. 29

3.1 Certesian coordinate used to study geomagnetic storm. Gm is for Geomagnetic meridian which is equivalent to the earth's horizontal magnetic field ($H = -Dst$). The southward magnetic field (B_{south}) causing geomagnetic storms due to the earth's North magnetic field component (B_x). This is the fact that northward variation is much greater than the eastward variation ($\Delta B_x >> \Delta B_y$) 37

4.1 The yearly-averaged number of sunspots visible on the sun from 1950–2009. The two vertical lines are to show the correlation of SSN with the severe geomagnetic storms. 41

4.2 Hourly Dst-index graph for the March 13–14, 1989 extreme geomagnetic storm, plotted for three days 42

4.3 Daily-disturbance storm time (Dst) index graph on March 1989 at a particular time of 2 hours. 43

4.4 Three consecutive days of hourly Dst-index graph for the October 29–31, 2003 geomagnetic storm 44

4.5 Three consecutive days of hourly Dst-index graph for the Nov.20–21, 2003 geomagnetic storm. It is followed by quiet phase, sudden storm commencement (SSC), storm main phase (SMP), and storm recovery phase (SRP) 45

4.6 Earth's surface impedance as function of angular frequency. The parameters used are $\omega = 0.0006 - 0.06\frac{rad}{sec}$, $\sigma = 0.001\frac{S}{m}$ and $\mu_\circ = 4\pi \times 10^{-7}\frac{H}{m}$ 46

4.7 The penetration depth as function of frequency. The parameters used are $\nu = 0.0001 - 0.01Hz$, $\sigma = 0.001\frac{s}{m}$ and $\mu_\circ = 4\pi \times 10^{-7}\frac{H}{m}$ 47

4.8 Graph of diffusion current density as function of inward distance(z) to the earth's center for different time instant of angular distance(ωt): a, b, c, d and e indicates for $\frac{\pi}{4}$, $\frac{\pi}{3}$, $\frac{\pi}{2}$, π and 2π radians; frequency(ν): 0.002, 0.004, 0.006, 0.008 and 0.010 Hz; period(T): 500, 250, 167, 125 and 100 seconds; angular frequency(ω): 0.01, 0.03, 0.04, 0.05 and 0.06 $\frac{rad}{sec}$; time instant(t): $\frac{T}{8}$, $\frac{T}{6}$, $\frac{T}{4}$, $\frac{T}{2}$ and T respectivily. 48

Acknowledgements

First of all, I would like to thank Almighty God and his son Jesus Christ for providing me wisdom, the ability and opportunity to prepare this thesis. Secondly, I would like to express my sincere gratitude to my advisor and instructor Dr. Remudin Reshid for his continuous guidance and great support.

I would like to extend my thanks to the department of physics of Addis Ababa University and all of my instructors, and to the Addis Ababa Education Bureau for their financial support during my MSc studies. I am also grateful to my colleagues especially to Ephrem, Kiflom, Abel, Murad and Jemal for their guidance, comments and feedbacks.

Last but not least, I would like to thank my parents who support me. I would also need to thank my wife Fikirte Bekele and my kid Hundket Debela for their love, inspiration and encouragement during preparing this thesis.

Addis Ababa University — Debela Alemayehu Gashe

October, 2020

Abbreviations

CMEs	=	Coronal mass ejections
ICMEs	=	Interplanetary Coronal mass ejections
SOHO	=	Solar and Heliospheric Observatory
ACE	=	Advanced Composition Explorer
NASA	=	National Aeronautics and Space Administration
EUV	=	Extreme Ultraviolet
STEREO	=	Solar TErrestrial RElations Observatory
SEPs	=	Solar energetic particles
OSO-7	=	Seventh Orbiting Solar Observatory
SMM	=	Solar Maximum Mission
LASCO	=	Large Angle Spectrometric Coronagraphs
SECCHI	=	Sun Earth Connection Coronal and Heliospheric Investigations
EUVI	=	Extreme ultraviolet imager
HI	=	Heliospheric Imager
MLSO	=	Mauma Loa Solar Observatory
Dst	=	Disturbance storm time
SSC	=	Storm Sudden Commencement
GICs	=	Geomagnetically Induced Currents
GPS	=	Global Positioning System
GMDs	=	Geomagnetic disturbances
ESP	=	Earth Surface Potential
FOV	=	Field of view
IMF	=	Interplanetary Magnetic Field
MHD	=	Magnetohydrodynamics

COR	=	Coronagraphs
HF	=	High frequency
IRIS	=	Interface Region Imaging Spectrograph
AU	=	Astronomical Unit
SMEI	=	Solar Mass Ejection Imager
WDC	=	World Data Center
SIDC	=	Solar Influences Data analysis Center
SSN	=	Sunspot number
CDAW	=	Coordinated Data Analysis Workshop
CACTus	=	Computer Aided CME Tracking Catalogue
AIM	=	Aeronomy of the Ice in the Mesosphere
TIMED	=	Thermosphere-Ionosphere-Mesosphere Energetic and Dynamics
THEMIS	=	Time History of Events and Macroscale Interactions during Substorms
IBEX	=	Interstellar Boundary Explorer
TRACE	=	Transition Region and Coronal Explorer
RHESSI	=	Reuven Ramaty High-Energy Solar Spectroscopic Imager
CINDI	=	Coupled Ion Neutral Dynamic Investigation
TWINS	=	Two Wide-Angle Imaging Neutral-Atom Spectrometers

Physical Constants

Permittivity of free space ($\varepsilon_\circ$)	=	$8.85 \times 10^{-12} \frac{c^2}{Nm^2}$
Speed of light (C)	=	$3.00 \times 10^8 \frac{m}{s}$
Permeability of free space ($\mu_\circ$)	=	$4\pi \times 10^{-7} \frac{H}{m}$
erg	=	$10^{-7} J$
Boltzmann constant (K_B)	=	$1.38 \times 10^{-23} JK^{-1}$
nanotesla (nT)	=	$10^{-9} T$

Symbols

g	=	acceleration due to gravity
ω	=	angular frequency
ν	=	frequency
σ	=	conductivity
ρ	=	resistivity or density
K_B	=	Boltzmann constant
$R_\odot$	=	Solar radii
nm	=	nanometers
nT	=	nanotesla

Abstract

In this thesis work we study coronal mass ejections (CMEs) and their impact on earth with emphases on solar active regions, geomagnetic storms and geomagnetically induced current densities. Based on present concept, strong southward interplanetary magnetic field and high-speed of interplanetary CMEs are important main drivers of severe geomagnetic storms that lead to geomagnetically induced currents. These can cause powerful effect on the magnetosphere to ground and on the modern technologies, such as power transmissions, satellites and spacecrafts, positioning and navigation systems, oil and gas pipe lines and harmful to astronauts in space. Therefore, primarly understanding for the prime drivers of the above effects in general is important, to predict space-weather and CME impacts on earth. We correlated sunspot cycle, CMEs and geomagnetic storms using yearly sunspot-index number data in the years of 1950–2009 and disturbance storm time index (Dst-index) data obtained from the WDC of Kyoto, Japan on March 12–14, 1989 and on October 29–31, 2003 to November 19–21, 2003. The results indicates that major CMEs can cause severe geomagnetic storms as on March 13–14, 1989 with Dst-index of $\sim -589nT$ during sunspot cycle 22 (1986–1996) of maximum sunspot number. On the other hand, during October 29–31, 2003 geomagnetic storm of minimum peak Dst-index of $\sim -400nT$ is correlated with the declining phase of sunspot number in cycle 23 (1996–2008). Moreover, we suggested that severe geomagnetic storms which affects modern technologies can be occured during the declining sunspot number (in the way of recovery phase) as well as during the maximum sunspot number (storm main phase). Finally, we computed sample of ground current densities using plane wave method, based on magnetic diffusion equation. We found that maximum amplitudes of this at the ground. Then, they all show an exponentially decrease in the intensity of current density values towards the earth center. Furthermore, we suggested that such east-west current densities during major CMEs can cause problem on power transmissions which are connected to area of high ground resistivity.

CHAPTER 1
Introduction

Sun is a provider of energy and life on earth. However, expulsions of magnetized plasma from its outer region is hazardous. That is, the sun is the source of intermittent ejections of bulk plasma and magnetic field structures called coronal mass ejections (CMEs). With space probes these structures are observed as they propagate in the interplanetary medium. Interplanetary coronal mass ejections (ICMEs) that have been detected by in situ instruments are identified by a combination of plasma and magnetic field parameters [1]. Recent studies have also suggested that, the sun is the source of the most powerful expulsions from the solar corona known as coronal mass ejections (CMEs). They generally erupt when twisted magnetic fields in the corona become unstable against the sun's gravitational field. Although the most of ejected materials are from solar corona, the primarly energetic magnetic sources are from chromospheric or photospheric origin. Moreover, a chance of CME belows directed at earth depends on its angular breadth, speed, strength, orientation and 11-year sunspot cycle. CMEs are best observed in white-light coronagraphs such as the Large Angle and Spectrometric Coronagraph onboard the Solar and Heliospheric Observatory (SOHO) which records photospheric light scattered by coronal electrons. In white light CMEs usually consist of a bright core and a cavity surrounded by a bright compression front. The cavity is believed to correspond to an expanding flux rope that is an integral part of a CME eruption [2].

In coronagraphic images, a CME can be recognized as bright features moving to progressively larger heliocentric distances. The movement is such that the lower part of the feature is always connected to the sun, that is the CME is anchored to the sun and it expands into the interplanetary space. The outward motion implies a finite speed of the CMEs and the motion from rest implies acceleration. The CME occupies a portion of the coronal images indicating a finite angular extent and hence defines a finite quantity of matter expelled from the sun [3, 4]. They often

propagate far into the interplanetary medium impacting planetary atmospheres and even the termination shock of the heliosphere. The magnetic fields embedded in CMEs can merge (interact) with earth's magnetic field, resulting in severe geomagnetic storms, which have serious consequences throughout the geospace and even for life on earth [4, 5, 7].

Magnetized plasma from the solar corona can then propagates across interplanetary space and envelop the earth. Satellites and spacecraft must therefore be designed to have a high level of resilience to these events, but the effects of the erupted material can also penetrate the magnetic fields and atmosphere that surround our planet, reaching down and into the surface of the earth, causing geomagnetic disturbance. These effects can then disrupt and sometimes damage a wide range of everyday technological systems that are often critical to the smooth functioning of modern societies [7, 8, 9].

The CME phenomenon was discovered in 1971, and still subject to investigation because it is the most important energetic phenomena that impacts throughout the heliosphere to the earth's magnetosphere [3, 6]. They represent an important source of magnetized plasma that follows sunspot cycle. Generally, CMEs are interest for both scientific and technological reasons. Scientifically they are interest because they remove built-up magnetic energy and plasma from the solar corona and technologically they are interest because they are responsible for the most extreme space weather effects at earth as well as at other planets and spacecraft throughout the heliosphere. Interplanetary CMEs are the main drivers of severe geomagnetic storms which can cause powerful effect on the magnetosphere to ground [3]. So that, these facts provide us the basic motivations for our study. Moreover, understanding the connection of solar storm and geomagnetic storm that affect human activities can then help us to protect our space based and ground based technologies. Sunspot cycle and disturbance storm time index are then useful for recognizing the CMEs prime cause for severe geomagnetic storms which in turn rise geomagnetically induced current (quasi-dc current) responsible for disruptions to normal power systems.

The general objective of this thesis work is to explore coronal mass ejections (CMEs) and their active source regions as well as their potential to cause severe geomagnetic storms throughout magnetosphere to the earth. Thus we are aimed to analyse CMEs as a prime cause for severe geomagnetic storms using sunspot number (SSN) and disturbance storm time index (Dst-index); and to compute local ground current densities using plane-wave method, based on magnetic diffusion equation.

The organization of the thesis will be as follows:- Chapter two deals with CMEs basic review and their impact on the earth. The basic parts of the sun and its active source region, CMEs observations, properties, and their theoretical models, as well as geomagnetic storm impacts are discussed in this chapter. In chapter three we present the data sources, analytical approach to fields, and methods for analysis of CMEs as a prime cause for geomagnetic storms. In chapter four the main results and discussions of the study are presented. Finally, conclusions of our work is presented in chapter five.

CHAPTER 2

CMEs basic review and their impact on the earth

2.1 An overview of the sun and its active regions

Understanding the nature of our sun is not only important for the scientists, but through better space weather predictions it makes a significant impact on our everyday life in our technology-dependent life in the 21^{st} century [10]. It is dynamic, continuously undergoing change, currently balancing the forces of nature to keep itself in equilibrium ($\nabla P = -\rho g$). That is, based on hydrostatic equilibrium, upward and downward forces must be balanced. Where ∇P is gradient of the gass pressure, ρ is density of the gass, and g is for the sun's gravitational field. The sun, like all stars, is an enormous ball of extremely hot, largely ionized gas (plasma), shining under its own power. Einstein's equation of $E = mc^2$ realized that the conversion of mass (m) into energy (E) is the source of the sun's heat and light. It does not have a solid surface or continents like earth, nor does it have a solid core. However, it does have a lot of structure and can be discussed as a series of layers. The fact that our sun is made up of mostly hydrogen (73%) and helium (25%) was first shown in a brilliant thesis in 1925 by Cecilia Payne-Gaposchkin, the first woman to get a PhD in astronomy in the United State [11].

Our sun is then active star that produces a variety of solar activities, such as sunspots, solar flares, prominences, coronal holes and coronal mass ejections (CMEs). In this section, we give an overview of the huge changes that occur in the sun's interior and atmosphere, the dynamic, violent eruptions of magnetized plasma and their associated solar activities.

2.1.1 The sun's interior

Three important developments over the last 30 years have enabled the physics of the solar interior to be studied in remarkable detail: these are through mathematical models of the sun, observations of solar vibrations, and observations of solar

neutrinos. Mathematical models use the laws of physics to predict about interior of the sun. The solar vibrations result from movement of gas within the sun, which generates waves of pressure that travel through the sun like sound waves moving through air. We can observe these vibrations on the sun's surface by looking for Doppler shifts. Light from portions of the surface that are rising toward us is slightly blueshifted, while light from portions that are falling away from us is slightly redshifted [12]. Solar neutrinos is the third way to study the sun's interior is to observe neutrinos released in the nuclear reactions or subatomic particles made by fusion reaction in the centre of the sun. Based on the above evidence, the sun's interior layer is usually separated into three regions: the core, radiative zone, and convective zone as discussed below (see Fig.2.1).

1. The core

   The solar core (extends upto $0.25R_{\odot}$) is the central part of the sun where nuclear fusion is transforming hydrogen into helium (the source of sun's energy). The energy produced by fusion in the core must then travel through many successive layers to the solar photosphere before it escapes into space as sunlight or kinetic energy of particles. At the sun's center the temperature is about 15 million K, the pressure is 200 billion times that on the surface of the earth [13].

2. Radiative zone

   Outside of the core, radiative zone (from about 0.25 to $0.70R_{\odot}$) where the thermal radiation is the most efficient means transporting intense energy generated in the core (in the form of high energy photons) outward. The energy generated in the core is carried by light (photons) that bounces from particle to particle through the radiative zone. Although the photons travel at the speed of light, they bounce so many times through this dense material that an individual photon takes about a million years to finally reach the interface layer. Photons emitted in the nuclear reactions are absorbed and re-emitted or scattered frequently so that their motion can be described as random. The temperature drops from about $7 \times 10^6 K$ at the bottom of the radiative zone to $2 \times 10^6 K$ just below the convective zone [13].

3. The tachocline

   The radiative zone and convective zone are separated by a thin layer known as the tachocline. This thin layer has become more interesting in recent years

as more details have been discovered about it. It is now believed that the sun's magnetic field is generated by a magnetic dynamo in this layer.

4. The convective zone

   The convective zone is the outer layer of the sun (from 0.70 to about $1.0R_{\odot}$). The temperature of the convective zone is lower than that in the radiative zone and haevier atoms are not fully ionized. Material heated the tachocline pick up heat and expand. This reduces the density of material and allows it to rise. Thermal convection carry the majority of the heat outward to the sun's photosphere. The materials cools off at the photosphere, which increases its density and causes it to the base of the convective zone. At the convective zone it picks up more heat from the top of the radiative zone and the cycle continues.

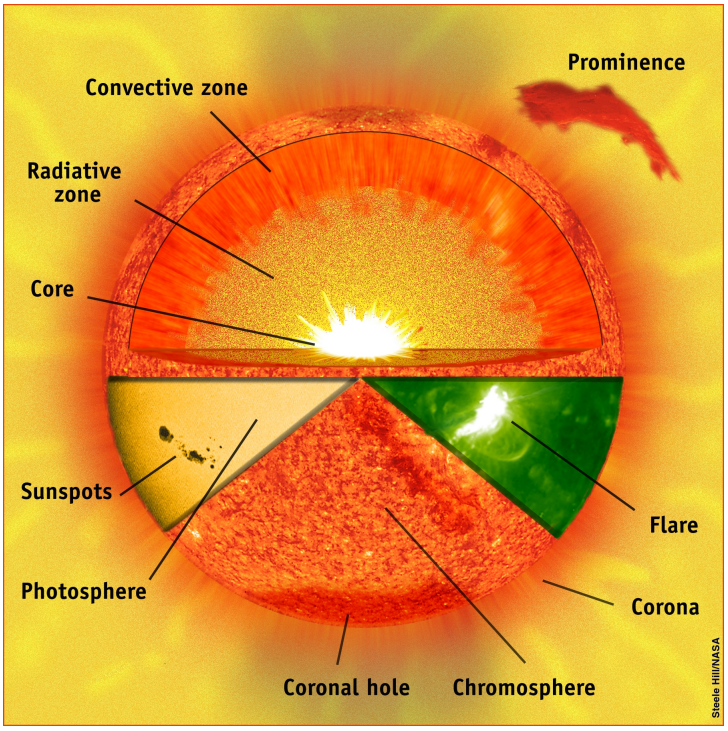

Figure 2.1: A basic overview of the parts of the sun (from SOHO images of the sun)

2.1.2 The sun's atmosphere

Based on their density, temperature, and composition the sun's atmosphere is usually separated into photosphere, chromosphere, transition layer and corona. However, the sun's atmosphere is a simplification as the atmosphere is an in homogeneous mix of different plasma properties due to up-flows, heating, cooling and

other dynamic processes. The temperature decreases in the photosphere, slowly rises at the top of chromosphere until there is rapid increases at the corona [13].

1. The photosphere

   The photosphere is the lowest layer of the sun's atmosphere that becomes opaque to visible light. The temperature of the photosphere averages just under 6000 K, and its surface seethes and churns like a pot of boiling water. The photosphere is where we find sunspots and regions of intense magnetic fields. Astronomers have found that the solar atmosphere changes from almost perfectly transparent to almost completely opaque in a distance of just over 400 kilometers; it is this thin region that we call the photosphere, a word that comes from the Greek to a lightsphere. When astronomers speak of the diameter of the sun, they mean the size of the region surrounded by the photosphere. Spectroscopic observation of the photosphere within and around the bright regions shows that direct evidence for the upward motion of gas as it boils up from within. This evidence proves that convection really does occur at or below the photosphere.

2. The chromosphere

   The chromosphere is the middle layer of the solar atmosphere and the region that radiates most of the sun's ultraviolet light. Analysis of the light produced in the chromosphere indicates that the gas density drops by more than a factor of 10^4 and that the temperature begins to increase with increasing altitude, from 4400 K to about 10,000 K. Normally the chromosphere is not visible, because its radiation is so much weaker than that of the photosphere. However, during total solar eclipses, the chromosphere shines into view for a few seconds at both ends of the total phase, when the moon hides the photosphere completely. The chromosphere then appears as a thin reddish sickle or ring. During eclipses the chromospheric spectrum, called the flash spectrum, can be observed. It is an emission line spectrum with more than 3000 identified lines. Brightest among these are the lines of hydrogen, helium and certain metals. One of the strongest chromospheric emission lines is the hydrogen Balmer α line at a wavelength of 656.3nm. Since the Hα line in the normal solar spectrum is a very dark absorption line, a photograph taken at this wavelength will show the solar chromosphere.

3. Transition region

   Outside chromosphere layer, there is a transition region of a few thousand kilometres, where the chromosphere gradually goes over into the corona. In the outer parts of the transition region, the kinetic temperature is already about $10^6 K$. This transition region may be selectively observed at various altitudes in the ultraviolet and extreme ultraviolet parts of the electromagnetic spectrum. In 2013, NASA launched the Interface Region Imaging Spectrograph (IRIS) to study the transition region to understand better how and why this sharp temperature increase occurs. IRIS is the first space mission that is able to obtain high spatial resolution images of the different features produced over this wide temperature range and to see how they change with time and location [11].

4. The solar corona

   The solar corona is the outermost layer of the sun's atmosphere which extends several million kilometers above the visible surface of the sun. It is region to a variety of dynamic and highly energetic activity, the cause of which is the build-up and release of magnetic energy. Of all the activity taking place in the corona, the most dramatical apparent of energy release is the coronal mass ejection (CME). It is characterised by low densities and its temperature is dramatically high-about 1 million K explaining why this region emits most of the sun's x-rays. The coronal plasma and the magnetic field move together, which is commonly known as frozen-in condition. If the magnetic field or the plasma is the dominant part can be expressed by the plasma β, defined as the ratio between the plasma pressure and the magnetic pressure:

$$\beta = \frac{P}{P_{mag.}} = \frac{nK_BT}{\frac{B^2}{2\mu_\circ}} \tag{2.1}$$

   where n is the particle number density, $\mu_\circ$ is the permeability of free space ,K_B is the Boltzmann constant and T is plasma temperature. In the corona $\beta << 1$, this indicates that the magnetic field dominates the plasma.

   Therefore coronal structure is controlled by solar magnetic fields, which form the corona into features called coronal streamers. The solar corona has a total visible brightness about equal to a full moon. Hence, since it is near the sun ($\sim 2-4R_\odot$), it is normally invisible, but can be observed during a total eclipse of the sun or by using a special type of telescope, called a coronagraph, that can block out the light from the solar disc (see Fig.2.2).

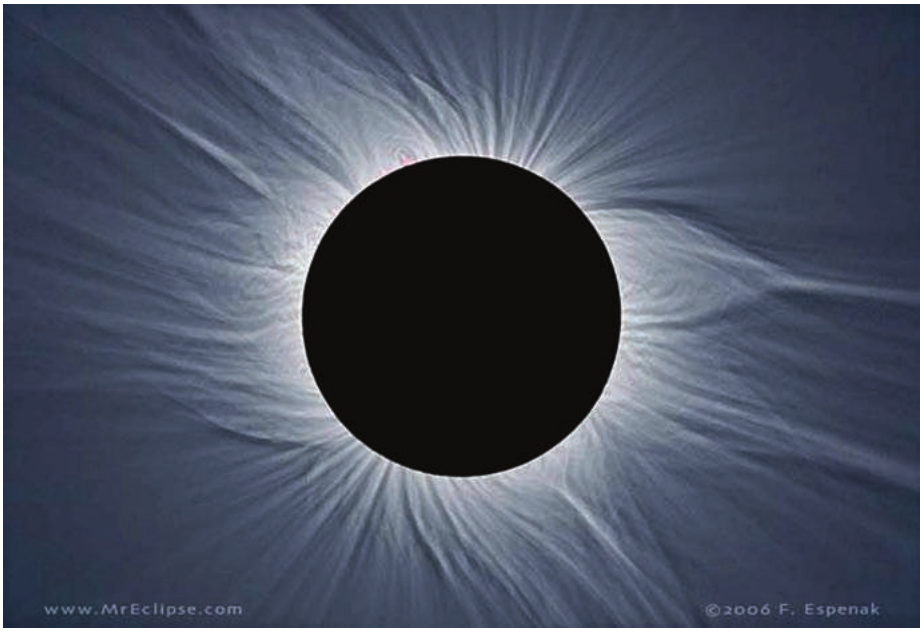

Figure 2.2: The solar corona at a time close to solar minimum (Image: Fred Espernak)

The x-ray emission from different coronal regions is very different. It is generally larger in regions of large sunspot groups. Coronal holes are regions on the solar surface where the x-ray emission is so small that the x-ray photograph looks dark. They have actually nothing to do with holes, but are just too cool or have too low densities to emit x-rays. They occur mainly in regions of open field lines which reach very far out from the sun before they close, and from which matter can more easily escape from the solar surface than in regions with closed field lines, i.e. in the loops. The density varies depending on the feature, such as the open magnetic structures of coronal holes can have densities in the region of $(0.5 - 1.0) \times 10^{14} m^{-3}$, streamers have densities in the region of $(3 - 5) \times 10^{14} m^{-3}$ while active regions have densities in the region of $(0.2 - 1.0) \times 10^{15} m^{-3}$. Coronal holes have the lowest temperature (less than $1 \times 10^{6} K$) followed by quiet sun regions at $(1 - 2) \times 10^{6} K$. Active regions are the hottest at $(2 - 6) \times 10^{6} K$ with flaring loops reaching even higher temperatures. The high temperatures reached in the corona give rise to EUV and x-ray emission, which have highly ionised iron lines as a prominent feature.

In the nineteenth century, scientists observed a spectral line at 530.3nm in the sun's outer atmosphere, called the corona. This line had never been seen before, and so it was assumed that this line was the result of a new element found in the corona, quickly named coronium. It was not until 60 years later that astronomers

discovered that this emission was in fact due to highly ionized iron. The visible corona during eclipses is due to Thomson scattering of photospheric light from free electrons in the coronal plasma. Based on the radiation coming from the corona, it has a number of components:

- The K-corona (from Kontinuierlich, the German word for continuous) produces the continuous white light emission that results from photospheric radiation scattered by free electrons. Contributions to the coronal light due to the K-corona primarily occur between 1 and $2.3R_{\odot}$ from the center of the sun. The spectral lines evident in the photosphere are essentially blended by the large Doppler shifts that are caused by the high thermal velocities of the electrons [13, 14].

- The F-corona (for Fraunhofer) comes from the scattering of photospheric light dust grains that are located beyond $2.3R_{\odot}$. Because dust grains are much more massive and slower than electrons. Doppler broadening is minimal and the Fraunhofer lines are still detectable. The F-corona actually merges with the zodiacal light, the faint glow found along the ecliptic that is a reflection of the sun's light from interplanetary dust [13, 14].

- The E-corona (Emissions) is the source of the emission lines that are produced by the highly ionized atoms located throughout the corona; the E-corona overlaps the K-and F-coronas. Some of the strongest lines are Fe xiv 530.3nm (green-line; visible), H-α at 656.3nm (visible), and Lyman-α121.6nm (UV). Since the temperatures are extremely high in the corona, the exponential term in the Saha equation encourages ionization because thermal energies are comparable to ionization potentials. The very low number densities also encourage ionization since the chance of recombination is greatly reduced [13].

- The T-corona (Thermal) is composed of thermal radiation from heated dust particles. It is a continuous spectrum according to the temperature and colour of the dust particles [13, 14].

2.1.3 Heating of the chromosphere and corona.

The most dramatic weathers and storms on the sun show that because of the sun's chromosphere and corona. But why this that gas so hot in the first place? Remember that temperature gradually decrease from the sun's core to the top of

its photosphere. But in referses the chromosphere and corona are much hotter than the sun's surface. Some aspects of this coronal heating remain mystrey today, but we have at least a general explanation:-The sun's magnetic fields carry energy upwards from the churning solar surface to the chromosphere and corona. More specifically, the rising and falling of gas in convection zone probabily shakes tightly wound magnetic field lines beneath the solar surface. The magnetic field lines carry this energy upward to the solar atmosphere, where they deposit this energy as heat [15]. The other is wave heating, in which sound, gravitational or magnetohydrodynamic waves are produced by turbulence in the convection zone. These waves travel upward and dissipate in the corona, depositing their energy in the ambient gas in the form of heat [16, 17].

2.1.4 Solar activity in the photosphere: sunspots.

CMEs have a wider implications for the solar dynamo because they reflect transient activity from sunspot and non-spot (quiescent filament) magnetic regions. Sunspots play an important role in the activity of the sun as they are the source of solar flares and many CMEs. That is, sunspot regions produce the most energetic CMEs because of the higher magnetic energy available [18].

It was Galileo who made the first telescopic observations of sunspots. Many spots become much larger than earth. Individual sunspots come and go, with lifetimes that range from a few hours to a few months. Sunspots usually come in groups with two sets of spots. One set will have north magnetic field while the other set will have south magnetic field. The key to understanding sunspots lies in their strong magnetic fields. This is why they appear dark against the photosphere. The darkest portion of the sunspot is known as the umbra. The umbra is usually surrounded by a less dark region is called the penumbra (see Fig.2.3). The existence of a strong magnetic field can be verified by observing individual spectral lines produced within the spot. Magnetic field strengths of several tenths of a tesla and greater have been measured in the centers of umbral regions, with field strengths decreasing across penumbral regions. Furthermore, polarization measurements indicate that the direction of a typical umbral magnetic field is vertical, becoming horizontal across the penumbra [19].

The other observable features in the photosphere is granulation (see Fig.2.3). Granules are small-scale features made up of brighter regions isolated by darker lanes interpreted as the upflow of hot material to the surface which then flows horizontally

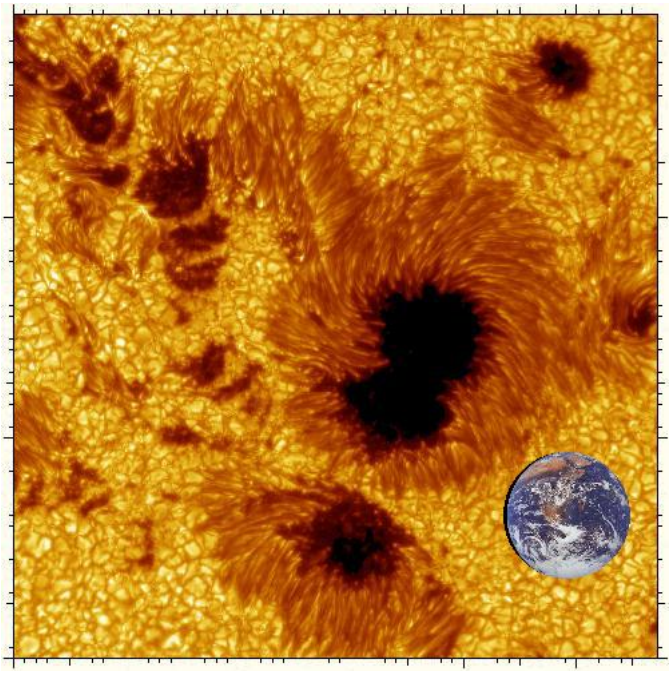

Figure 2.3: Photo of a sunspot on the solar surface:NASA/courtesy of nasaimages.org.

and cools, flowing back down in the dark lanes. Each granule measures about 1,000 km across, is as deep as the photosphere, and has a lifetime of between 5 and 10 minutes. Each granule forms the topmost part of a solar convection cell.

2.1.5 Magnetism and solar cycle

The number of sunspots and their position relative to the equator is a periodic phenomenon with a period of approximately 11 years that is commonly called the solar cycle. This is due to the inversion of the polarity of the sun's magnetic field over that period. During the solar cycle, the sunspots migrate towards the solar equator (see Fig.2.4 top) and the number of sunspots on the solar surface also varies with time with a period of 11 years (see Fig.2.4 bottom). The period for a complete cycle during which the solar magnetic field polarity returns to its original configuration is approximately 22 years (N to S to N) [20].

Figures showing the migration of the sunspots over time such as Fig.(2.4 top) are often called butterfly diagrams since the shape of the sunspot distribution in these figures resembles the wings of a butterfly. They are also sometimes called Maunder's butterfly diagrams that are named after the British astronomer Edward W. Maunder. At the beginning of the cycle sunspots tend to appear on disk with a latitudinal distribution of $\pm 30^{\circ}$ of the equator. As the cycle progresses, sunspots

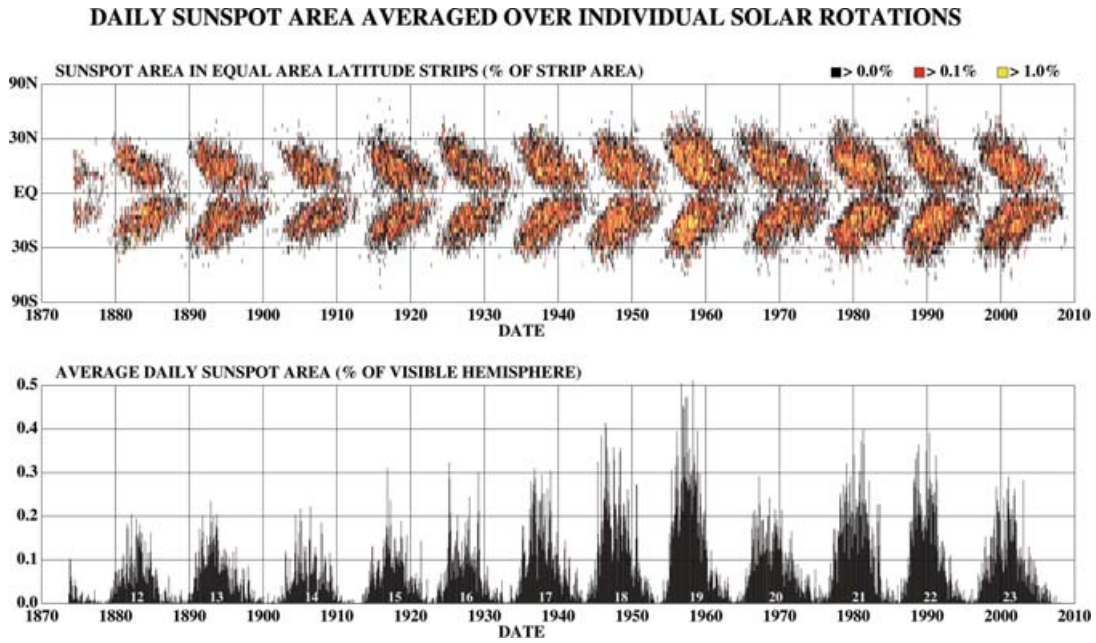

Figure 2.4: Sunspot cycle during the past century (Image: courtesy of NASA MSFC)

appear at lower and lower latitude, until they eventually disappear at the end of a cycle. The Fig.(2.4 bottom) shows how the number of sunspots on the sun changes with time. The vertical axis shows the percentage of the sun's surface covered by sunspots. The cycle has a period of approximately 11 years.

The activity of the sun in the form of active regions, flares, prominences and coronal mass ejections follows the sunspot cycle with these events being most common at solar maximum and least common at solar minimum. Over the course of a solar cycle, the sun changes polarity at the time of sunspot maximum. For example, an overall dipolar configuration of North-South will become South-North, another cycle will bring it back to North-South once more (one full magnetic cycle takes 22 years). The complex behavior of the solar magnetic field over an 11 year activity cycle, during which the dipole reverses sign, is generally explained by solar dynamo theory [21].

Why is the sun such a strong and complicated magnet? Astronomers have found that it is the sun's dynamo that generates the magnetic field. In the sun, the source of kinetic energy is the churning of turbulent layers of ionized gas within the sun's interior. These generate electric currents (moving electrons) which in turn generate magnetic fields.

2.1.6 Differential rotation of the sun

The sunspots follow the magnetic lines that are distorted by the differential rotation of the sun. Sun does not rotate as a rigid sphere. The equator of the sun rotates faster than the poles of the sun. This is called the differential rotation. Sunspots and many other solar activities are due to this differential rotation. Differential rotation plays a crucial role in the understanding of solar activity and the solar dynamo. The twisting action creates the solar dynamo and an 11-year solar cycle of magnetic activity, as the sun's magnetic activity reverses it self every 11 year (see Fig.2.5).

By measuring Doppler shifts at the solar limb, we find that the sun rotates differentially (that is, the rate of rotation depends on the latitude being observed). At the equator the rotation period is approximately 25 days, increasing to 36 days at the poles. Observations of solar oscillations have showed that the sun's rotation also varies with radius. Near the base of the convection zone, the differing rotation rates with latitude converge in a region known as the tachocline. The strong shear that is set up in this region is believed to result in electric currents in the highly conducting plasma, which in turn generate the sun's magnetic field. Thus, the tachocline is probably the source of the sun's magnetic field.

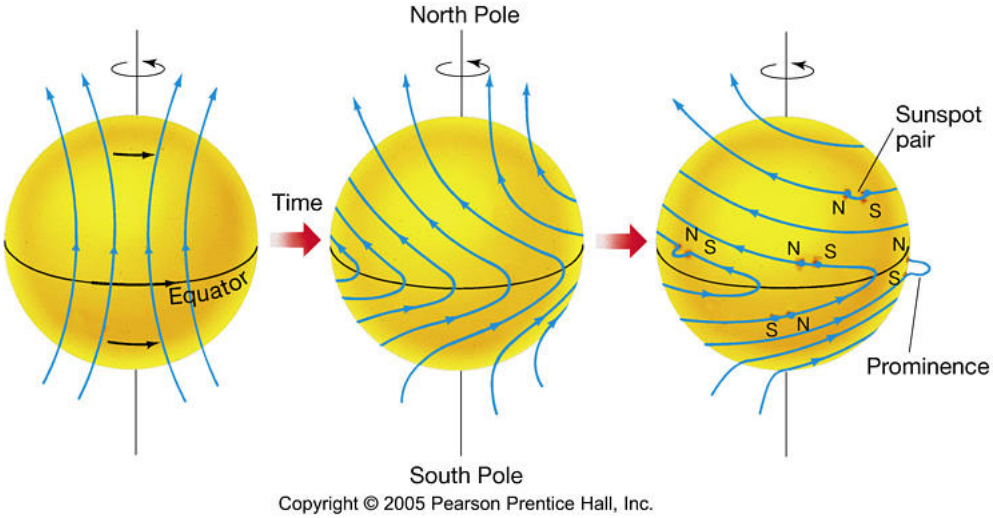

Figure 2.5: The sun rotates more quickly at its equator than it does near its poles. Because gas circles the sun faster at the equator, it drags the sun's north-south magnetic field lines into a more twisted configuration. The magnetic field lines linking pairs of sunspots, depicted here as dark blobs, trace out the directions of these stretched and distorted field lines [15]

2.1.7 Solar activity above the photosphere: prominence and flare

The discovery that eruptive prominences or filaments are substructures of CMEs has helped extend CME studies back to the mid-1800s. Prominences were first seen probably during total solar eclipses, but only some sporadic observations were made before the 19^{th} century, describing them for example as burning holes or red flames. Quiescent prominences are one of the largest individual magnetic features on the sun. They often end their existence through an eruption as part of a coronal mass ejection (CME). Prominences are located in the solar corona and consist of plasma that has parameters comparable to that of the chromosphere they are cold and dense compared to the surrounding corona.

Solar flares are violent explosions, observed as sudden brightenings in the solar atmosphere above active regions (sunspot groups). They take place in the chromosphere and the corona, but the strongest ones can heat up even the photosphere (producing flare visible even in white light). The first solar flare was observed in 1859 by Richard Carrington, who was drawing sunspots, when he suddenly noticed two bright spots in one of the sunspot groups.

2.2 Coronal mass ejections (CMEs)

Coronal mass ejections (CMEs) are massive expulsions of plasma and magnetic flux from the solar corona. Fast CMEs can drive shocks in the corona and interplanetary space, which are key accelerators of solar energetic particles (SEPs). Characterizing the shock three-dimensional (3D) geometry, kinematics and their connection with heliospheric impacts is of crucial importance for space weather research and forecasting. They represent an important source of solar variability from the point of view of plasma and magnetic field. They remove billions of tons of magnetized plasma from the sun and dump them into the sun-earth connected space once every other day during solar minimum and several times per day during solar maximum. CMEs also provide dramatic variable energy input to the magnetosphere, in addition to and sometimes in combination with the high speed streams that originate from coronal holes. CMEs are the source of major disturbances in the interplanetary medium and can be directly observed up to $32R_{\odot}$ from the sun [22].

A modern understanding of CMEs tells us that they are large-scale eruptions of plasma and magnetic field that propagate from the low solar corona into interplanetary space. They have speeds in the range $\sim 10^2 - 10^3 kms^{-1}$, masses of $10^{13} - 10^{16}$g,

and kinetic energies of $10^{29} - 10^{32}$ergs, making them the most energetic explosive events in the solar system and a major cause of adverse space weather in the near-earth environment [23, 24]. Recent studies of coronal mass ejections (CMEs) also shows that they are large-scale structures of magnetized plasma that are expelled from the sun with speeds ranging from some 100 up to about $3500kms^{-1}$, driven by magnetic forces. They are the most energetic events in our solar system, being associated with energy releases of up to some 10^{32}ergs. Fast CMEs are often associated with EUV waves, which are widely believed to be low-coronal signatures of large-amplitude fast-mode magnetosonic waves or shocks. When the interplanetary CME (ICME), and its associated shock reaches earth, they may induce strong geomagnetic storms, with the storm strength mainly depending on the southward (B_z) component of the ICME's magnetic field and on its impact speed. Recent studies, in particular owing to the multi-spacecraft in-situ observations of the STEREO satellites, revealed the production of wide-spread solar energetic particles (SEPs), which seem to be able to fill the whole heliosphere. It is understood that these extreme cases of wide-spread SEP events are either related to specific properties of the CME and its associated shock close to the sun (extended source region) and to perpendicular particle transport processes in interplanetary space. Thus, the understanding of the origin and early evolution of CMEs close to the sun, their interplanetary propagation as well as their interaction processes with the earth's magnetosphere are all key aspects in the understanding and prediction of extreme space weather events [25].

2.2.1 A brief history of CMEs

The first recognized space weather event was the so called Carrington event in 1859 when an intensive white-light solar flare was observed for the first time and followed by an intense and broad-range terrestrial responses. These terrestrial responses included low-latitude aurorae, as well as the arcing from the induced currents in the telegraph wires in USA and Europe [26]. The event aroused much speculation on a causal link between the phenomena Carrington observed on the sun and the magnetic activity recorded throughout the earth. It was not until 1919 that a theory was put forward to suggest plasma transients emitted from the sun may impact the earth and cause geomagnetic activity and the aurora [27]. Up until the 1940s, the only evidence confirming the plasma transient hypothesis was the correlation between solar and geomagnetic activity. However, following the development of radio receiver technology during World War Two, much interest

was given to solar radio bursts and their indication that disturbances travel away from the sun at speeds of up to $500kms^{-1}$. Further evidence came from the fields of cosmic ray studies, when it was suggested the ground level detections of particles at earth, such as those reported by Forbush in 1946, may be related to the acceleration of particles by a shock moving through the solar atmosphere. Eventually this activity was summarised by Gold in 1962, who hypothesised the expulsion of magnetized plasma from the solar atmosphere, and the driving of a shock by this expulsion that accelerates particles into interplanetary space, nowadays this hypothesis is still subject to investigation, given that flares may be responsible for high energy particles that accompany eruptive events [28, 29].

Gold's paper marked over 100 years of indirect evidence for the expulsion of the plasma transients from the surface of the sun toward earth. However, it was not until December 14, 1971 that the first direct images of one of these plasma expulsions was made with the coronagraph onboard the 7^{th} Orbiting Solar Observatory (OSO-7) satellite. This marked the beginning of white-light CME studies as we know them today, and it was followed by a number of other instruments, including Skylab, P78-1 (Solwind), and the Solar Maximum Mission (SMM), which provided coronagraph observations up until 1989. The modern era of CME observations began in 1995 with the launch of the Solar and Heliospheric Observatory (SOHO) and its more sophisticated suite of instruments, including the Large Angle Spectrometric Coronagraphs (LASCO). In 2006 LASCO was joined by the coronagraphs onboard the Solar Terrestrial Relations Observatory (STEREO) and together they provide observations of CMEs from the low solar atmosphere into interplanetary distances [30].

Therefore, the beginning of the space era and the development of scientific satellites and spacecraft, a huge amount of data was collected, both in situ in the interplanetary medium and from remote sensing of the sun. This allowed the observation, study of CMEs properties, a confirmation of what was first postulated by Carrington and discovery of many solar and interplanetary phenomena that we know today.

2.2.2 Observations of CMEs

Observations of the corona and CMEs are possible only when the photosphere of the visible sun is occulted. Such occultation occurs naturally during solar eclipses and is artificially created by spaceborne coronagraphs. A coronagraph produces an artificial solar eclipse. It uses an occulting disk to block the sun's bright surface,

revealing the faint solar corona, stars, planets and sungrazing comets. Coronagraphs view the outward flow of density structures emanating from the sun by observing photons emitted from photosphere Thomson-scattered by free electrons in solar corona.

1. Space-based observations

   A number of orbital coronagraphs were flown in space which provided better data and longer periods of CME observations. Spaceborne coronagraphs which observed CMEs include OSO-7 coronagraph in the early 1970s, Skylab (1973–1974), P78-1 (Solwind) (1979–1985) and Solar Maximum Mission (SMM) (1980; 1984–1989). In late 1995, the Solar and Heliospheric observatory (SOHO) was launched and it is located along the sun-earth line in the point of equilibrium between the gravity of the earth and the sun (L1 Lagrangian Point), about 1.6×10^6 km distant from the earth (see Fig.2.6). The Large Angle Spectrometric Coronagraph (LASCO) is one of the instrument sets onboard SOHO. It consists of three white-light coronagraphs, called C1 ($1.1-3R_\odot$), C2 ($1.5-6R_\odot$) and C3 ($3-32R_\odot$). Together the instruments cover from $1.1-32R_\odot$. Two of the three LASCO coronagraphs (C2, C3) are still operating and C1 ceased operation in June 1998.

   The Solar-Terrestrial Relations Observatory (STEREO) is a set of two identical spacecraft, one located ahead and the other behind the earth when taking into consideration the orbit around the sun. Both spacecraft are located at about 1 Astronomical Unit (AU) distant from the sun. The spacecraft ahead is referred as STEREO A and the one behind as STEREO B. Among other instruments onboard STEREO, the CMEs can be studied using a set of five instruments called sun-earth connection coronal and heliospheric investigation (SECCHI). The acronym was chosen as a reference to the Italian astrophysicist Angelo Secchi (1818–1878), one of the pioneers to photograph the sun during eclipses. SECCHI has three types of instruments. One is an extreme ultraviolet imager (EUVI) telescope that allow us to study the solar chromosphere and the solar corona up to $1.7R_\odot$. The second type is a white-light coronagraph, which is a more accurate observational estimation of both CME kinematics and CME mass, resulting in a better understanding of CME dynamics. Each one of the twin STEREO spacecraft has two coronagraphs, called COR1 and COR2. Together they cover the corona from $1.4-4R_\odot$ and from $2.5-15R_\odot$, respectively. They are very similar to the C2 and C3 coronagraphs from the

LASCO instrument. The third type of instruments is called Heliospheric Imager (HI), covers the corona from $12 - 84R_{\odot}$ (HI1) and $66 - 318R_{\odot}$ (HI2). These coronagraphs are designed to provide 3-D view of CMEs in the inner and outer corona [31, 32].

2. Ground-based observations

   Ground-based instruments for imaging corona are complementary to the space-based ones because they can achieve a better temporal resolution and are not limited by the telemetry rate. However, they are limited by the intensity and temporal variability of the sky. The main operating ground based coronagraphs today include the Mauna Loa Solar Observatory (MLSO) K-coronameter ($1.2-2.9R_{\odot}$) and the green line coronagraphs at Sacramento Peak, New Mexico and Norikura [33].

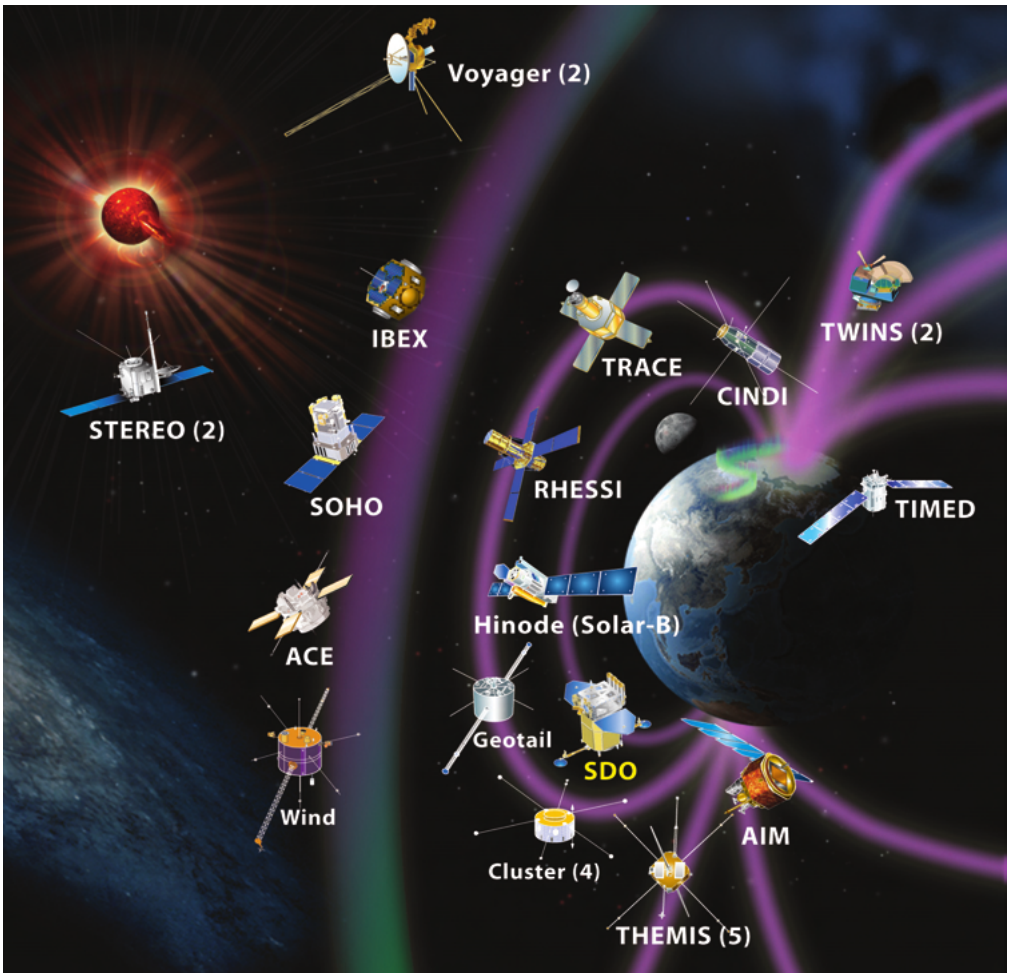

Figure 2.6: Some spacecraft obsevatory in the heliosphere that studying the sun and the sun-earth environment [34]

.

From Fig.(2.6), we see that each heliophysics system observatory has their own missions:- SOHO/LASCO, earth-directed CMEs monitor; STEREO/SECCHI, to investigate 3D-CMEs structure; ACE, measures the electron-protons that are send by solar wind; Geotail, study the processses through which solar wind energy, momentum, and particles must pass to enter the magnetosphere; IBEX, explore the interstellar boundaries beyond the solar system; Voyager, explore the intraction of the heliosphere with the local interstellar medium; Wind, explore the large-scale structure of global interplanetary disturbances in the inner heliosphere; TRACE, explore 3D-magnetic structures in the solar atmosphere; RHESSI, investigate energy release in the solar flares; Hinode, investigate the sun's magnetic field and how energy stored in the field is released; SDO, observe how the sun's magnetic field is generated and structured in its interior and how stored magnetic energy in the corona is released into the heliosphere; Cluster, explore the micro-and meso-scale dynamic of magnetospheric phenomena; THEMIS, understand the substorm instabilities that abruptly and explosively release solar wind energy stored within the earth's magnetotail; AIM, discover the causes of polar mesospheric clouds and their relationship to climate change; CINDI, explore the dynamics of the earth's ionosphere; TWINS, investigate the nature of sources, transport, and sinks of plasma populations; TIMED, explore solar cycle-induced variability of the thermosphere, ionosphere, and mesosphere [34].

2.2.3 Properties of CMEs

The measured properties of CMEs include their occurrence rates, locations relative to the solar disk, angular widths, speeds and accelerations, masses, and energies. There is a large range in the basic properties of CMEs, although some of this scatter is likely due to imaging projection effects. If a CME is not exactly at the solar limb, its derived properties will be an underestimate and the width an overestimate. Recent developments using auxiliary data and the multiple viewpoint capability of STEREO have attempted to overcome this problem [35, 36].

1. Morphological properties of CMEs

   CMEs are most often observed using a coronagraph, an instrument that obscures the bright solar disk so the much fainter corona can be imaged. Some of the observed CMEs appear as a three-part structure (see Fig.2.7), with a bright leading edge, followed by a dark cavity (void) and a bright core. The void is supposed to be a region of high magnetic field and less plasma

density. In some CMEs the void region appears to have a flux rope structure and exhibit a clear three-part structure. The central bright core structure is the prominence material that erupts along with the CME. The bright leading edge (front) is interpreted as where a coronal plasma is pileup. The front may contains swept-up as well as primary material. Although this CME is regarded as typical in appearance, many CMEs do not have all of these features and some appear to have more complex morphological structures, with only around 30% of all CMEs exhibiting the three part structure. The varied nature of their appearance and morphology can usually be attributed to projection effects, that is the CME is a 3-D object projected onto a 2-D image, hence its appearance depends on its orientation in the corona. Fundamental difference can be found between narrow CMEs and normal CMEs. The narrow CMEs show jet-like motions probably along open magnetic field, on the other hand normal CMEs are characterized by a closed frontal loop. There are also CMEs without a bright core (loop CMEs). Some arise from pre-existing coronal streamers (the so-called streamer blowouts), while others appear as wide almost global eruptions [37, 38].

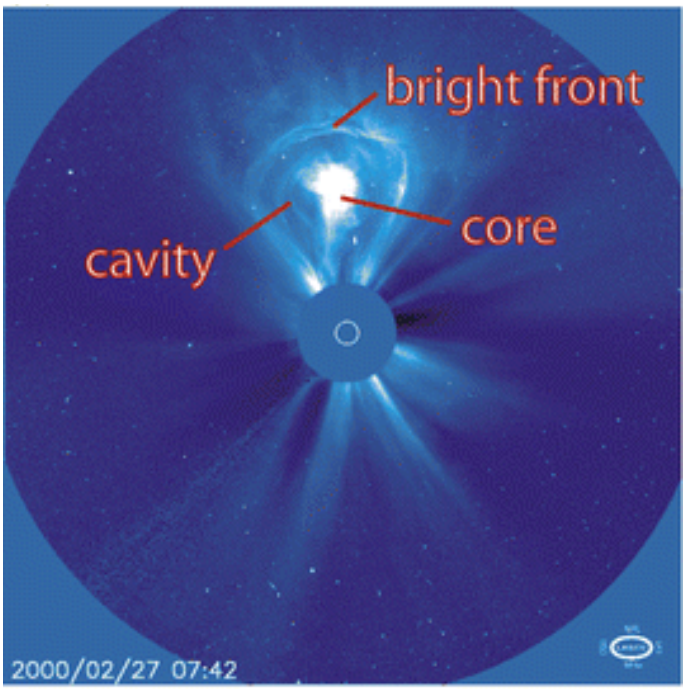

Figure 2.7: A three-part CME with the core, cavity, and bright front marked (Credit: SOHO/ LASCO CME Catalog)

2. Kinematic properties

   A coronagraph at plane of sky or limb CME (one that erupts on the solar limb and propagates at right angles to the observer-sun line), offers the best measure of their apparent angular widths, speeds, acceleration, etc.

   - CME speeds and acceleration

     Estimates of the apparent speeds of the leading edges of CMEs range from about $20 - 2500 kms^{-1}$. The annual average speeds of Solwind and SMM CMEs varied over the solar cycle from about $150 - 475 kms^{-1}$. On the other hand, LASCO CME speeds did generally track sunspot number in solar cycle 23, from 280 to $\sim 550 kms^{-1}$. For a typical CMEs, above a height of about $2R_{\odot}$ the speeds are relatively constant in the field of view of coronagraphs. The slowest CMEs tend to show acceleration while the fastest tend to decelerate. This can be expected, considering that CMEs must push through the surrounding solar wind, believed to have a speed of around $400 kms^{-1}$ in the outer corona.

     CMEs typically accelerate fast in the low corona until gravity and other drag forces slow them further out. This process continues into the interplanetary medium. The early acceleration for most CMEs occurs low in the solar corona ($< 2R_{\odot}$). Only 17% of all LASCO CMEs experience acceleration out to $30R_{\odot}$. Lawrence, Dennis and others have identified the strong acceleration using LASCO data found that gradually accelerating CMEs looked balloon-like in coronagraph images, but fast CMEs moved at constant speed even as far out a $30R_{\odot}$. Sheeley found that when viewed well out of the sky plane, gradual CMEs looked like smooth halos which accelerated to a limiting value then faded, while fast CMEs had ragged structure and decelerate. In the LASCO field of view slow CMEs tend to accelerate and fast CMEs decelerate, while those around the solar wind speed having constant speeds [31].

   - Angular width

     The angular width of CMEs projected in the plane of the sky ranges from $\sim 2^{\circ} - 360^{\circ}$, with a significant fraction in the low end ($< 20^{\circ}$) and a small fraction in the high end ($> 120^{\circ}$). CMEs with angular widths less than $\sim 10^{\circ}$ can be called narrow CMEs, and others are sometimes called normal CMEs. The average width of LASCO/SOHO CMEs is found to be 40° for limb CMEs. The average width is relatively smaller (47°)

during solar activity minimum compared to that during solar maximum ($61°$). Halo CMEs, with an apparent angular width of or close to $360°$, are simply due to the fact that the CMEs propagate near the sun-earth line, either toward or away from the earth. Halo CMEs appear to surround the occulting disk in the sky plane projection. In reality, these are like any other CME, except that they expand rapidly and more energetic beyond the extent of the occulting disk [35].

- Frequency occurence

  The frequency of CME observation depends strongly on the phase of the 11-year solar cycle. During solar minimum around one is observed per day, nearly five per day are observed at solar maximum. During solar cycle 23 (1996–2008), LASCO observations provided unprecedented observations of CMEs. The occurrence rate of CMEs was found to largely track the solar activity cycle, but with a delay of 6–12 months between the solar cycle maximum and maximum occurence rate of CMEs. Before the launch of SOHO, the average occurrence rate was found to increase from 0.2 per day at solar minimum to 3.5 per day at solar maximum. With the increased sensitivity and wider field of view, the SOHO/LASCO coronagraphs detected CMEs more frequently. The CDAW catalog lists around 13,000 CMEs identified visually. The results from this catalog suggest that the CME occurence rate increases from ~ 0.5 per day near solar minimum to ~ 6 near solar maximum. However, the automated software, CACTus3, identified many more events for the same period, with the occurrence rate increasing from <2 per day near solar minimum to ~ 8 per day near solar maximum [35, 36].

3. CME mass and kinetic energy

   The mass is estimated from coronagraphic images as the excess mass above the pre-event corona. The mass below the occulting disk is not included. Each CME is assigned a single mass value, which is the mass attained in the outer corona after an initial increase with time, similar to the CME width. CME mass calculations require a conversion from the coronagraph observed intensity to electron (and therefore plasma) density using the physics of Thomson scattering. Masses and energy calculations of CMEs require difficult instrument calibrations and often suffer from significant uncertainties. The older coronagraph data (Skylab, SMM and Solwind) derived the average mass

of CMEs to be a few times 10^{15}g. Calculations using LASCO observations indicate a slightly lower average CME mass, 1.6×10^{15}g. This is because LASCO can measure smaller masses down to the order of 10^{13}g. Studies using Helios and LASCO data suggest that the older CME masses may have been underestimated. This is because mass outflow may continue well after the CME's leading edge leaves the instrument field of view. The true mass calculations using the STEREO data states that the CME mass increases with time and height then reaches a constant value above about $10R_{\odot}$. The kinetic energy ranges from about 10^{26} to 10^{33}erg, with an average value of 2.0×10^{29}erg [39].

It is a difficult task to measure CME masses and energies using white light images farther from the sun. This is because of the lack of calibration information and the uncertainties imposed by the faintness of the CMEs compared to the background noise. The 3-D density reconstructions of a few CMEs observed in the heliosphere by SMEI also give the mass and energy estimates. These mass estimates generally agree with the mass of the same CMEs as derived from LASCO data. The kinematical properties, mass calculations are based on coronagraph images and, therefore, subject to the same problems of projection and perspective. More recent work making use of the stereoscopic capabilities of STEREO have provided more accurate measurements.

2.2.4 Theoretical CMEs models

The objective of every model is to induce a loss of equilibrium of the structure, but the mechanism by which this is done varies greatly amongst the models. Storage models assume a slow build up of magnetic stress in a non-potential field that may store free energy over long time scales before some loss of equilibrium occurs and the stored magnetic energy is rapidly converted to mechanical energy and the expulsion of a magnetic structure [40]. Dynamo models involve a rapid generation of magnetic flux by either stressing of the field or flux-injection into the system. As the name suggests, these models usually consider the interplay between current and magnetic field in the system that may bring about a Lorentz force which provides an expulsion of the flux rope from the low corona [41]. The most important models we used to study CMEs are discussed here:

1. Catastrophe model

   The catastrophe model assumes a flux-rope is formed in the corona before eruption and considers the balance between magnetic tension holding the flux rope in position, and magnetic pressure (from compression of field lines under the rope) that supply an outward directed force. A loss of equilibrium is brought about by photospheric motions, either convergence or shearing of the foot points, which are well-known precursors to eruptive activity in the corona. Continued contraction results in a magnetic compression that eventually dominates tension, resulting in a flux rope rise (see Fig.2.8). As the rope rises it forms a current sheet behind it, and its evolution after this point depends on whether or not reconnection occurs in the current sheet. If no reconnection is present then the flux rope simply rises and finds a new equilibrium position at a greater height, in this case the net release of magnetic energy is less than 1% of the energy stored in the pre-field configuration. If reconnection occurs, then the eruption proceeds uninhibited and up to 95% of the stored magnetic energy is released [42].

2. Magnetic breakout model

   The magnetic breakout model involves multipolar magnetic flux system. An essential requirement for the breakout model is that the coronal magnetic topology is due to a multipolar flux distribution at the photosphere and that it contains at least one null point where reconnection can occur [44]. A core magnetic field is flanked by two side-lobe fields, which collectively lie underneath an overarching field that stabilizes the whole system (see Fig.2.9). The overarching field and core field are almost anti-parallel, creating a magnetic null point between the two. Non-potentiality is injected into the core by twisting or shearing of the foot points or by flux emergence. This non-potentiality causes the core field to grow and encounter the overarching field, distorting the null point into a current sheet and eventually allowing reconnection to occur. The reconnection removes field lines from the overarching field and adds it to the side-lobe systems, allowing further growth of the core field. The growth of the core field in turn drives further breakout reconnection resulting in a positive feedback required for explosive expulsion of the core. Finally, as the core is accelerated a current sheet forms in its wake, eventually leading to a separation of the core flux from the solar surface that forms a plasmoid structure typical of a three part CME [45].

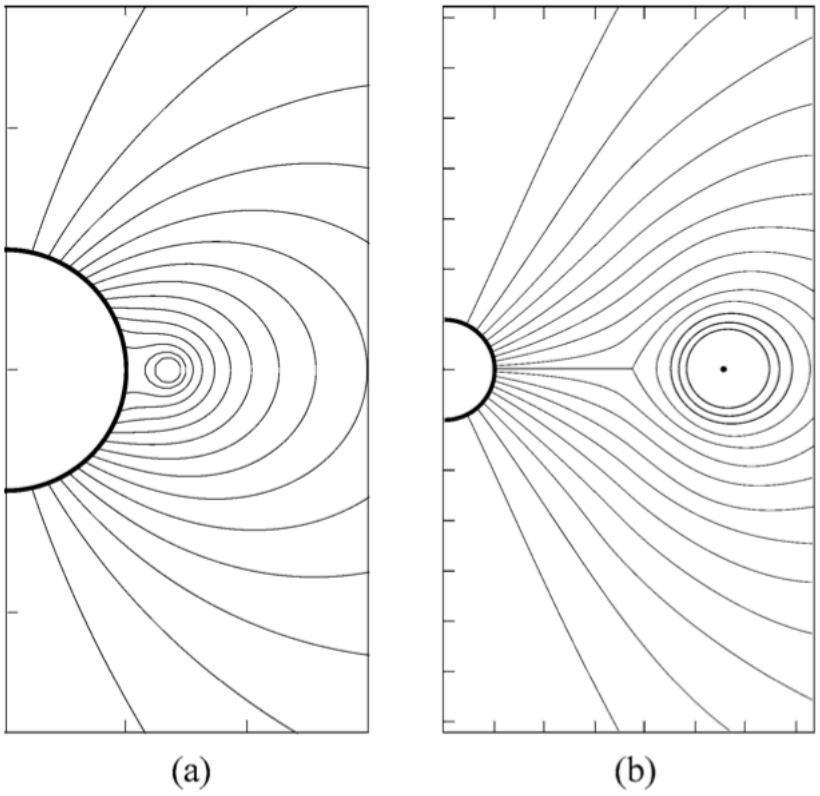

Figure 2.8: Flux cancellation model showing the erupting flux rope at two different heights. a) Close to the sun flux rope is in equilibrium and b) at a larger distance it is unstable against gravitational pull of the sun. Here, a current sheet is formed beneath the flux rope [43].

2.3 CMEs-Geomagnetic storm impacts

The most earth-impact solar disturbances are named coronal mass ejections (CMEs) in causing severe geomagnetic storms. Geomagnetic storms can then defined as disturbances of earth's magnetosphere caused by the interplanetary CMEs. Interplanetary CMEs are the primary drivers of almost all space weather disruptions, including highly accelerated magnetized plasma and most major geomagnetic storms, with potential impacts on a wide range of human activities. The effect of earth directed coronal mass ejections (CME) from the sun reveals a sensational impact on the atmosphere and geosphere. The response of the magnetosphere to interplanetary shocks or pressure pulses can result in sudden injections of energetic particles into the inner magnetosphere. That is, during north-south component of the IMF directed downwards, more solar wind and energized plasma cause sudden magnetospheric compression or are allowed to enter the magnetosphere (see Fig.2.10). This process is called magnetic reconnection. As a result, energized plasma coming from

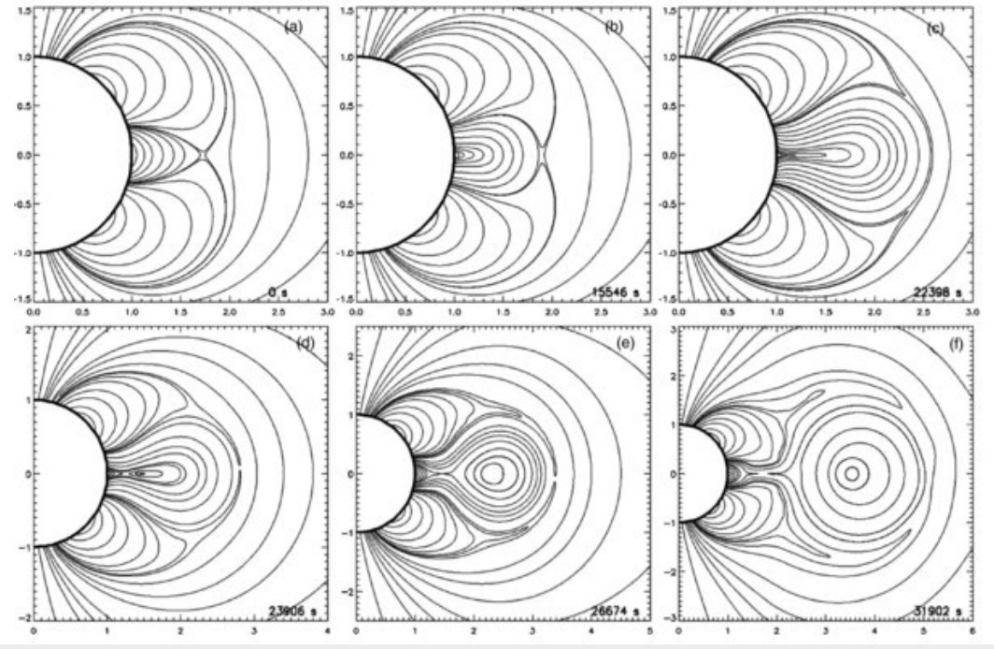

Figure 2.9: Magnetic field lines during the eruption process based on the magnetic breakout model. The flux rope system rises and reconnects with the overlying magnetic field lines. A current sheet is built behind an isolated flux rope and magnetic reconnection then leads to the eruption of the flux rope [45]

the magnetosphere may generate geomagnetic effects detectable in the geospace, upper atmosphere, ionosphere, and on the ground [46, 47, 48, 49, 50, 51, 52].

Scientists verified that there were a series of major solar storms occurring between March 13–14, 1989 on the surface of the sun. According to the reports published on geomagnetic storm of 1989, scientists identified major solar storm heading towards the earth on March 9, 1989 with a speed of a million miles per hour and hit the earth on March 13–14, 1989 causing severe disturbances in the earth's magnetic field. The March 1989 geomagnetic storm (the hydro-Quebec event) is one of the most well-known for its power blackout in Canada and North America [53, 54]. Another extreme geomagnetic storm caused by the impact of fast CME on earth is storms occured on the October 29–31, 2003 (the Halloween storms). These geomagnetic storms caused power blackout in Sweeden and severe damage to power grids in South Africa [51, 55].

2.3.1 Disruptions to electrical systems

When the magnetic field of a CME interacts with earth's magnetic field, there is a induced magnetic reaction here on earth. If the CME is a mild one, as most are, we

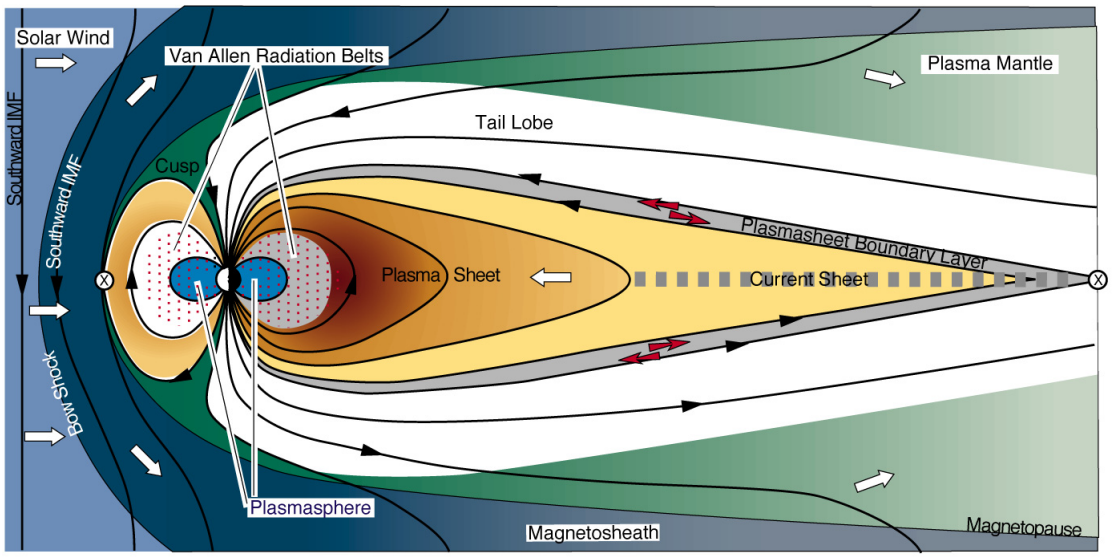

Figure 2.10: Earth's magnetosphere [48]

see the reaction as a strong aurora in the sky near the north pole which we would term an extended northern lights show. However, during severe solar storms, enormous amounts of energy are transferred to our magnetosphere which can create huge geomagnetically induced currents (GICs) running through the earth's surface and through the grid. The potential threat of geomagnetically induced current (GIC) on power system networks was fully appreciated after the complete blackout of March 13, 1989 in Quebec and some parts of North America. The geomagnetic variations in the earth's magnetic field induce voltages which produce GIC (quasi-dc currents) which have very slow variation in the frequency range of about 0.0001–0.1Hz. GIC enter the grounded neutral connected transformers causing transformer core cycle saturation. Frequency relays, which are not prepared for quasi-dc currents trip circuit breakers, and disrupt the normal power system operations.

High latitude areas are much more prone to solar disturbances. But recent studies have indicated that even the mid latitude and low latitude regions have some potential risk to geomagnetically induced currents. Recent reports of transformer equipment damage, relay tripping and other faults in power systems in South Africa, areas reasonably far from auroral zone, contradict conventional thinking. Since many African countries are located at the geomagnetic equator, where space induced currents (equatorial electrojet) are too high, such power plant damage is a real threat for the country. The geomagnetic disturbances are more pronounced

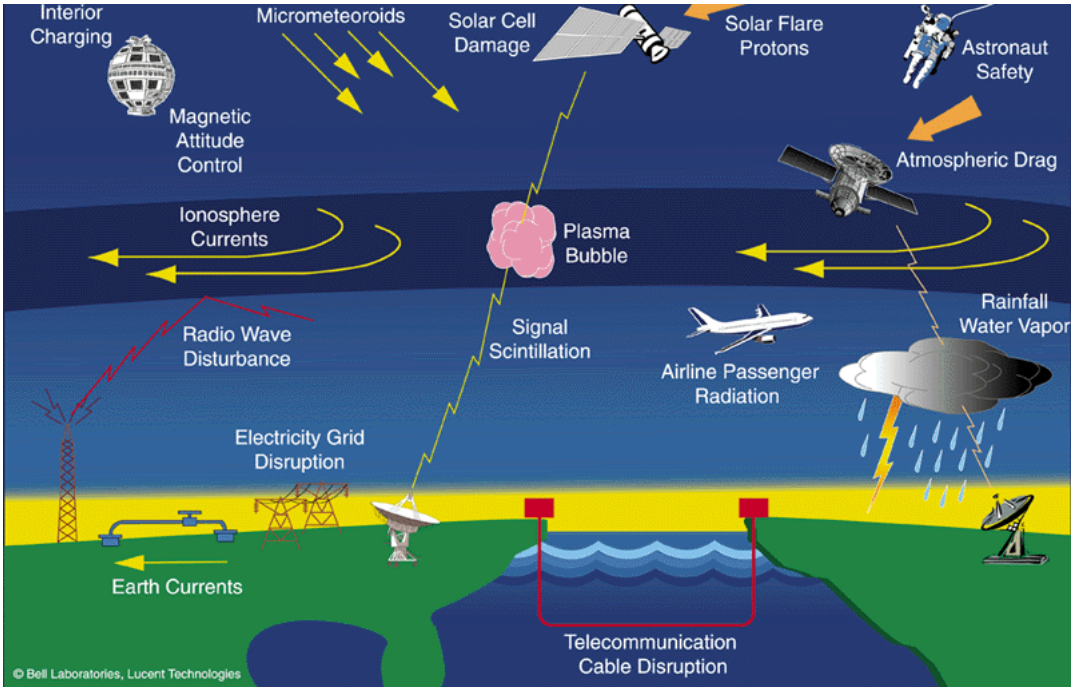

Figure 2.11: All of the above space based and ground based technologies, and geospace environment are disrupted durng severe geomagnetic storm [31].

in areas located around the igneous rock formations. The conductivity of the earth and geoelectric field is interrelated. The igneous rock formations with high resistivity and low conductivity are highly prone to geomagnetic disturbance [56, 57, 58, 59, 60, 61].

2.3.2 Problems in communications and navigation systems

High frequency (3–30MHz) communication systems use the ionosphere to reflect radio signals over long distances. Ionospheric storms can affect radio communication at all latitudes. Some frequencies are absorbed and others are reflected, leading to rapidly fluctuating signals and unexpected propagation paths. TV and commercial radio stations are little affected by solar activity, but ground to air, ship to shore, shortwave broadcast and amateur radio (mostly the bands below 30MHz) are frequently disrupted. Radio operators using HF bands rely upon solar and geomagnetic alerts to keep their communication circuits up and running.

Telegraph lines in the past were affected by geomagnetic storms. Telegraphs used a single long wire for the data line, stretching for many miles, using the ground as the return wire and fed with DC power from a battery; this made them susceptible to being influenced by the fluctuations caused by the magnetic storm. Today much

of communication for critical infrastructures are based on optical fibers which are not directly susceptible to GIC. However, there is still a substantial part of communications routed through copper wire and thus susceptible to GIC, which could lead to both temporary disruption of service and permanent damage to equipment [56, 57, 58, 59, 60]. GPS signals are affected when solar activity causes sudden variations in the density of the ionosphere, causing the GPS signals to scintillate. Airplanes and ships used the very low frequency signals from these transmitters to determine their positions. During solar events and geomagnetic storms, the system gave navigators information that was inaccurate by as much as several miles. If navigators had been alerted that a geomagnetic storm was in progress, they could have switched to a backup system [56, 57, 58].

2.3.3 Satellite hardware damage

Satellites and spacecrafts are especially sensitive to disturbed space weather since they cannot take advantage of the protection from earth's magnetosphere during severe geomagnetic storm. There is both a likelihood of equipment damage to the satellites and a likelihood of disruption of their communication (that is, particularly true for communication satellites and GPS signaling) due to disturbances in the ionosphere. Geomagnetic storm also causing satellites to slow and change orbit slightly. Skylab's 1979 destruction is an example of a spacecraft reentering earth's atmosphere prematurely as a result of higher than expected solar activity. During the great geomagnetic storm of March 1989, four of the Navy's navigational satellites had to be taken out of service for up to a week. During geomagnetic storms, the number and energy of electrons and ions increase. When a satellite travels through this energized environment, the charged particles striking the spacecraft differentially charge portions of the spacecraft. If sufficient charge accumulates in any one component, it may attempt to neutralize by discharging to other components. This discharge is potentially hazardous to the satellite's electronic. Certainly, astronauts in space and even airline passengers in high-flying transpolar routes can be adversely affected by solar storms and geospace disturbances. Austronauts are subject to potentially lethal doses of radiation. Penetration of high-energy particles into living cells can cause chromosome damage, cancer and other health problems (even death) [56, 57, 58, 59].

2.3.4 Problems in geologic exploration and hazard in pipelines

Earth's magnetic field is used by geologists to determine subterranean rock structures. For the most part, these geodetic surveyors are searching for oil, gas or mineral deposits. They can accomplish this only when earth's field is quiet, so that true magnetic signatures can be detected. Other geophysicists prefer to work during geomagnetic storms, when strong variations in the earth's normal subsurface electric currents allow them to sense subsurface oil or mineral structures [57, 58]. Geomagnetically induced currents (GICs) also affect oil and gas pipelines. In pipelines, GIC and the associated pipe to soil voltages can increase the rate of corrosion in pipelines especially in high latitude regions. Damage resulting from corrosion is cumulative in nature and can eventually lead to pipeline integrity failures and major fuel leaks [58, 60, 62].

2.4 CMEs and their impact: summary

Massive expulsions of plasma and magnetic flux from the solar corona are called coronal mass ejections (CMEs). They are best observed using the modern space probe satellites like LASCO onboard SOHO, and SECCHI onboard STEREO. The probability of CME belows directed at earth depends on its angular widths, speeds, and orientation with the earth's magnetosphere. Moreover, major CMEs follow sunspot cycle and then have earth effects on the sun to earth connections because they are major drivers of geomagnetic storms. Severe geomagnetic storms can then rise to give geomagnetically induced current (GICs) and have critical impacts on electric power supply, spacecraft and aviation industries, communications and navigation systems, oil and gas pipe lines, and harmful to astronauts in space (see Fig.2.11). Further evidence of geomagnetic storm impacts on power systems was recognised after March 1989 severe geomagnetic storms (the hydro-Quebic event). More evidence followed after October 2003 geomagnetic storms (the Halloween storms). Therefore, primarly understanding magnetically connections of solar storms and geomagnetic storms are very important to predict space-weather and CMEs impact on earth.

CHAPTER 3

Methods for analysis of geomagnetic storms and GICs during CMEs directed to the earth

3.1 CME-Geomagnetic storms

Statistically, CME-geomagnetic storms impact follow a 11-year sunspot cycle. Major solar storms occur during the maximum sunspot activity. These involve solar mass ejection and its orientation towards the earth (southward magnetic field) and the speed of the solar winds. The CMEs cause their own current and southward magnetic fields, can interact with the northward magnetic field of earth. This forms reconnection at the front side of the magnetosphere and in the magnetotail which is responsible for the coupling between the solar wind and earth's magnetosphere that drives the aurora and geomagnetic storms. That is, the solar wind transfers plasma, momentum and energy into the earth's magnetosphere. This in turn distorts the dipole of magnetic fields of the earth, compressing the dayside (sunward side) and drawing the nightside (anti-sunward side) out into a magnetotail. Furthermore, the existence of the ring current system in the earth's magnetosphere is then responsible for the reduction in the horizontal component of the geomagnetic field during the storm main phase. As reconnection takes place and then energy is released, charged particles originating from the solar wind enter deep into the magnetosphere. As a result currents are formed in the magnetosphere and ionosphere-ring current are increased forming eastward protons and westward electrons (auroral electrojet currents). The charged particles are then gradually store in the earth's radiation belts. These ring currents are the contribution of geomagnetic storm which is recorded by geomagnetic observatories [53, 51].

3.2 Phases and severity of geomagnetic storms

A geomagnetic storm has three phases: initial, main and recovery. The initial phase is characterized by Dst-index increasing by 20 to $50nT$ in tens of minutes.

The initial phase or warning phase is also referred to as a storm sudden commencement (SSC). However, not all geomagnetic storms have an initial phase and not all sudden increases in Dst-indices are followed by a geomagnetic storm. The main phase of a geomagnetic storm is defined by Dst-index decreasing to less than $-50nT$. The selection of $-50nT$ to define a storm is somewhat arbitrary. The minimum value during a storm will be between -50 and approximately $-600nT$. During the main phase of the storm, lasting hours to a day, the southward magnetic field in the cloud of solar particles makes contact with the earth's oppositely-directed northward-pointing magnetic field. These process in which the two fields join are called magnetic merging (reconnection), and then for a time the earth becomes magnetically connect to an active region on the sun. The recovery phase is when Dst-index changes from its minimum value to its quiet time value. The recovery phase may last as short as 8 hours or as long as 7 days [50].

More severe storms are expressed with the minimum negative value Dst-indices. The severity of geomagnetic storms are related with the orientation of earth's magnetic field in relation to the solar storm magnetic orientation. The size of a geomagnetic storm is classified as: a weak storm usually has a minimum Dst of $-30nT$; the moderate storm, $-50nT < Dst < -30nT$; the intense storm, $-100nT < Dst < -50nT$; and superintense geomagnetic storms, $-500nT < Dst < -100nT$ are relative- ly rare. The term extreme event (severe) is for storms with $Dst < -500nT$ [51].

3.3 Disturbance storm time index (Dst-index)

Geomagnetic storm intensities are measured by a very common index called disturbance storm time (Dst) index. The disturbance storm time (Dst) index, which is the average change in the earth's horizontal magnetic field brought about by the geomagnetic storm as measured in nT at four low-latitude stations, quantifies the intensity of the geomagnetic storm. The Dst-index has a time resolution of one hour and is compiled from measurements obtained by ground magnetometers at stations located in middle latitudes. Dst-index is the commonly used index today, for recognising CMEs responsible as a prime cause for geomagnetic storms [50].

3.4 Data sources for Dst-index and SSN

In this thesis we will use the disturbance storm time (Dst) index data obtained from the World Data Center (WDC) in Kyoto, Japan to study the intensity of the

geomagnetic storm. Geomagnetic storm measured by disturbance storm time (Dst) index is driven by the earthward CMEs during the maximum solar activity. The disturbance storm time (Dst) index is the average change of the earth's horizontal magnetic field in units of nT, located at the four middle latitude magnetic observatories namely Hermanus (HER), Kakioka (KAK), Honolulu (HON), and SanJuan (SJG). During a storm creates a stronger southward magnetic field it opposes the earth's magnetic field, and the effect is a net decrease in the measured field along the equator. This is why some records of geomagnetic storm strength by the ground magnetometers are in negative nanotesla. High negative Dst-index means severe geomagnetic storm. Dst-indices are sensitive to the ring currents. On the other hand, the sunspot number (SSN) data is the commonly used index of solar activity available from Solar Influences Data analysis Center (SIDC) in Royal observatory of Belgium, to study the dependency of geomagnetic storms on solar magnetism and 11-year sunspot cycle. Sunspots are much larger than the earth's surface. They are regions of intense magnetic field and source of solar storm. Each sunspots are one of the active region on the sun which can grow, decay and reorganize on lifetime of minutes to hours, hours to months, and collectively the spot emerge in groups that define the roughly 11-year activity cycle and 22-year magnetic activity of the sun. The typical solar wind speed, southward IMF and earthward coronal mass ejections vary with the cycle. Large earthward coronal mass ejections can cause extreme geomagnetic storms as occured in 1989 storm during cycle 22 and in 2003 storm during cycle 23. Thus, coronal mass ejections (CMEs) occur abundantly in the maximum solar activity, so we expect intense CME-related main phase geomagnetic storms during the maximum solar activity or in rising (declining) phase of the cycle.

3.5 Analytical approach to fields and GICs

Geomagnetically induced currents (GICs) are occured in the earth when coronal mass ejections (CMEs) on the solar corona send charged particles towards the earth. These particles interact with the earth's magnetic field causing what is known as a geomagnetic storm. So changes in the earth's horizontal magnetic field, usually expressed in nT, produce very small electric field variations. These in turn give rise to quasi-dc (frequency range of from about 0.0001–0.01Hz) currents in the solid body of the earth, and also in any man-made infrastructures that are electrically connected to earth [70, 71, 72].

Estimating the impact of CMEs on the earth requires understanding the geomagnetic field variations, the influence of the local ground conductivity, and the degree they produce geomagnetically induced currents (GICs). In principle, the concept of GIC is related with Faraday's law of induction ($\nabla \times E = -\frac{\partial B}{\partial t}$). That is, the changing horizontal geomagnetic field induce quasi-dc currents in the ground according to Ohm's law ($J = \sigma E$). GICs are commonly more intense at high latitude regions and in area of igneous rock geology. However, recent study has recognised that effects of GICs are not limited in high latitude regions, the effect is also occured in mid-low latitude regions [51].

Plane wave method is a well-established and widely used method of computing magnetic diffusion equation and ground current density. This section introduces the method of the magnetic diffusion equation used to calculate geomagnetically induced currents. Starting with the magnetoquasistatic approximation of Maxwell's equations wherein there is no wave propagation. Developing from the magnetoquasistatic approximation, geomagnetically induced electric fields and ground current density are obtained by solving the magnetic diffusion equations.

3.5.1 Magnetoquasistatic equations

For geomagnetically induced currents(GIC) of very low frequency range of about 0.0001–0.01Hz, the induced electric field is also varying slowly with time. The very slow time variation, displacement current in the Maxwell's equation, can be dropped so that the wave propagation equation does not have to be used [64, 65, 66, 67]. The omission of $\frac{\partial D}{\partial t} = \frac{\partial \varepsilon_\circ E}{\partial t}$ enables the magnetoquasistatic onto Maxwell's equations to be assumed. The relevant magnetoquasistatic equations are:

$$\nabla \times E = -\frac{\partial B}{\partial t} \tag{3.1}$$

$$\nabla \times H = J \tag{3.2}$$

$$\nabla \cdot D = 0 \tag{3.3}$$

$$\nabla \cdot E = 0 \tag{3.4}$$

and the constitutive relations

$$D = \varepsilon_\circ E, B = \mu_\circ H, J = \sigma E. \tag{3.5}$$

where J is the current density in $\frac{A}{m^2}$, $\mu_\circ$ is the magnetic permeability of free space in $\frac{H}{m}$, $\varepsilon_\circ$ is the permittivity of the free space in $\frac{F}{m}$, and σ is the ground conductivity in $\frac{S}{m}$.

3.5.2 Derivation of magnetic diffusion equation

Fundamentally, the physical concept of the flow of geomagnetically induced current (GIC) is associated with Faraday's law of induction, from Eqn.(3.1). That is, changing magnetic fields induce electric currents in conductors. For the range of conductivities within the earth and the frequencies of concern for geomagnetically induced current (GIC), $\sigma >> \varepsilon_{\circ}\omega$. We assume that every where $\mu_{\circ}$ has its free space value, $\mu_{\circ} = 4\pi \times 10^{-7}\frac{H}{m}$. For a very slow time variation of the field form $e^{i\omega t}$, and using the Eqn. (3.5) we can rewrite the first two equations.

$$\nabla \times E = -i\omega\mu_{\circ}H \tag{3.6}$$

$$\nabla \times B = \mu_{\circ}\sigma E \tag{3.7}$$

Taking the vector identity $\nabla \times (\nabla \times B) = \nabla(\nabla \cdot B) - \nabla^2 B$, and substituting for E from Eqn.(3.7) into Eqn.(3.6) gives the general magnetic diffusion equation

$$\nabla^2 B = i\omega\mu_{\circ}\sigma B \tag{3.8}$$

3.5.3 Physical set up of certesian coordinate

For the case of plane wave theory, we ignore the curvature of the earth's surface and establish the cartesian coordinate system in which the x-and y-axes are true northward and eastward respectively, and the z-axis is vertically down towards the centre of the earth (see Fig.3.1). We assume that the electric and magnetic fields induced by the space currents are plane waves propagating along the z-axis, and the ground is regarded as an infinite half-space with a uniform conductivity. The earth's surface is the x-y plane at z=0 with the z-axis pointing downwards [68]. During massive brust of magnetically charged material reaches above the earth, it changes magnetic fields which in turn induce electrical currents (electrojets) at above the surface of the earth. Thus, GICs are related to the intensity of the ionospheric current and its temporal or spatial variations flowing at about 110 km altitude (the equatorial electrojet). This electrojet encircles the earth above the equator flowing east to west.

3.5.4 Solutions of the magnetic diffusion equation

The solution of the magnetic diffusion equation in the ground using appropriate boundary conditions is related to space-field above it by satisfying the continuity of the magnetic fields at $z \geqslant 0$. For our assumptions, the solutions of the analysis

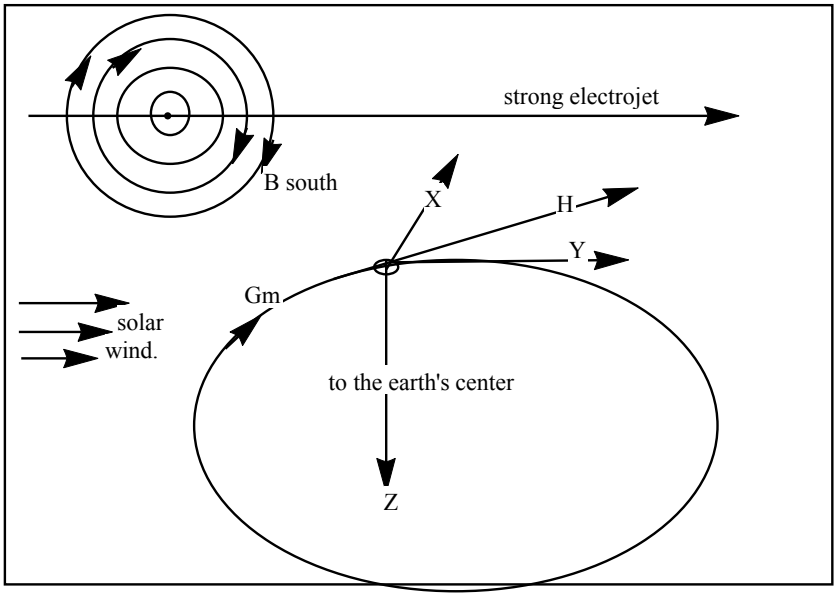

Figure 3.1: Certesian coordinate used to study geomagnetic storm. Gm is for Geomagnetic meridian which is equivalent to the earth's horizontal magnetic field ($H = -Dst$). The southward magnetic field (B_{south}) causing geomagnetic storms due to the earth's North magnetic field component (B_x). This is the fact that northward variation is much greater than the eastward variation ($\Delta B_x >> \Delta B_y$)

are valid in a small region close to the surface of the earth in the vicinity of the strong auroral or equatorial electrojet. The surface at z=0 is subjected to a spatially constant, but time-varying magnetic field in the x-direction. Thus, magnetic field induced by the strong electrojet is to be assumed as $B_{space} = B_x(z,t)$. Then , Eqn.(3.8) becomes:

$$\frac{d^2 B_x(z,t)}{d^2 z} = \sigma \mu_\circ \frac{dB_x(z,t)}{dt} \tag{3.9}$$

We seek a steady-state solution of Eqn.(3.9) for z>0, subject to appropriate boundary conditions at z=0, and whose z dependence decays exponentially at large z because of skin depth effect. The diffusion Eqn.(3.9) implies that there is only an x-component throughout the half-space, z>0 and it is a function of z and t.

Because the magnetic diffusion equation is second order in spatial derivatives and first order in the time, it is convenient to use complex notation, with the understanding that the physical fields are found by taking imaginary parts of the solutions. Thus, the plane wave solution form of Eqn.(3.9) is given based on [53] and the reference therein.

$$B_x(z,t) = B_\circ e^{kz} e^{i\omega t} \tag{3.10}$$

Where $B_\circ$ is the extreme value of the ground magnetic field strength and k is the

coefficient of z which is obtained by substituting Eqn.(3.10) into Eqn.(3.9), and equating the left hand-side to the right hand-side to obtain

$$k^2 = i\mu_\circ\sigma\omega \Rightarrow k = \pm(1+i)\sqrt{\frac{\mu_\circ\sigma\omega}{2}} \tag{3.11}$$

where k is induction wave number. The square root in the Eqn.(3.11) has the dimensions of an inverse length characteristic of the medium of the frequency. The length is called the skin depth or penetration depth (δ):

$$\delta = \sqrt{\frac{2}{\mu_\circ\sigma\omega}} \tag{3.12}$$

The depth of penetration into the earth by the upper magnetospheric-ionospheric source fields depends upon the frequency (ν) and the local ground conductivity. As the frequency decreases, the penetration depth will be increases and as the higher the conductivity, then the shallower the penetration. A skin depth concept is used for visualizing a compartition of the penetration of fields within a conductor.

From our assumption, $B_x(z,t)$ decays exponentially at large z, so we choose the negative value of induction wave number. By substituting the negative coefficient of z from Eqn.(3.11) into Eqn.(3.10) to obtain;

$$B_x(z,t) = B_\circ e^{(-i-1)\sqrt{\frac{\mu_\circ\sigma\omega}{2}}z} e^{i\omega t} \tag{3.13}$$

$$B_x(z,t) = B_\circ e^{-\sqrt{\frac{\mu_\circ\sigma\omega}{2}}z} e^{-i\sqrt{\frac{\mu_\circ\sigma\omega}{2}}z} e^{i\omega t} \tag{3.14}$$

and using the Eqn.(3.12), the above equation is reduced to;

$$B_x(z,t) = B_\circ e^{-\frac{z}{\delta}} e^{i(\omega t - \frac{z}{\delta})} \tag{3.15}$$

3.5.5 Ground current density and electric field

Since the field varies in time, there is an accompanying small electric field. From Ampere's Eqn.(3.2) and Ohm's law, together with the existence of only $B_x(z,t)$, we found that there is only a y-component of geomagnetically induced field (E), which is function of z and t given by:

$$E_y(z,t) = \frac{1}{\mu_\circ\sigma}\frac{d}{dz}B_x(z,t) \tag{3.16}$$

$$E_y(z,t) = \frac{1}{\mu_\circ\sigma}\frac{d}{dz}(B_\circ e^{-\frac{z}{\delta}} e^{i(\omega t - \frac{z}{\delta})}) \tag{3.17}$$

$$E_y(z,t) = (\frac{-1-i}{\mu_\circ\sigma\delta})(B_\circ e^{-\frac{z}{\delta}+i(\omega t - \frac{z}{\delta})}) \tag{3.18}$$

After using the identity, $\frac{1}{\delta\sigma} = \sqrt{\frac{\mu_\circ\omega}{2\sigma}} = \frac{\mu_\circ\omega\delta}{2}$ and the polar form with the help of Euler's formula for the complex part, we obtain the following equation.

$$E_y(z,t) = -\sqrt{\frac{\omega}{\mu_\circ\sigma}}B_\circ e^{-\frac{z}{\delta}}e^{i(\omega t+\frac{\pi}{4}-\frac{z}{\delta})} \tag{3.19}$$

The horizontal geoelectric field component at the earth's surface is related to the perpendicular geomagnetic variation component by the following equation.

$$E_y = -\sqrt{\frac{\omega}{\mu_\circ\sigma}}B_x e^{i\frac{\pi}{4}} \tag{3.20}$$

The electric field is modified by the magnetic diffusion equation so that E_y is dependent on the square root of the angular frequency and resistivity. In addition, there is a 45° phase shift between the geoelectric and geomagnetic fields. The electric field is associated with a localized current density.

$$J_y = \sigma E_y = -\sqrt{\frac{\sigma\omega}{\mu_\circ}}B_\circ e^{-\frac{z}{\delta}}e^{i(\omega t+\frac{\pi}{4}-\frac{z}{\delta})} \tag{3.21}$$

3.5.6 Earth's surface impedance

Geographical conditions are highly responsible for GICs have an effect on power transmission. Variable conductivities and rock formations increase the vulnerability to geomagnetic disturbances. The geomagnetic disturbances are more pronounced in areas located around the igneous rock formations. The igneous rock formations with high resistivity and low conductivity are highly susceptible to geomagnetic disturbance. If the power plant is located over igneous rock with low conductivity, any geomagnetic disturbance will cause a bigger change in the voltage it induces in the local ground.

If local ground conductivity is uniform, the relation between the electric and the magnetic fields at the earth's surface can be found from Eqns.(3.15) and (3.19).

$$Z(\omega) = \frac{E_y}{B_{space}} = \frac{\omega\delta}{\sqrt{2}} = \sqrt{\frac{\omega}{\sigma\mu_\circ}} \tag{3.22}$$

where $Z(\omega)$ is the magnitude of surface impedance in Ω and ω is the angular frequency in $\frac{rad}{sec}$.

The simplest electric field model is the uniform field approach, in which a constant electric field is assumed, with the magnitude given in the maximum electric field in units of about 1 volt per kilometre after the geomagnetic storm of March 1989. The induced potential ε between any two ground points, is obtained by evaluating the line integral of the geomagnetically induced electric field ($\varepsilon = \oint E\cdot d\ell = E_y\ell_y$). It depends on east-west distance (ℓ_y) and the local ground conductivity (σ), geomagnetic variations and the magnetospheric-ionospheric currents.

CHAPTER 4
Results And Discussion

1. Solar cycle, CMEs and Geomagnetic storm

   During a strong southward interplanetary magnetic field of sunspot activity phase, geomagnetic storm is occured which can be quantified by the disturbance storm time (Dst) index. Dst-index is the indication of the average change in earth's horizontal magnetic field. That is, Dst-index values give the average deviation of the earth's horizontal magnetic field from its normal value. This is occured when southward magnetic field and speed of interplanetary magnetic field cause geomagnetic storm. The relation of Dst-index, southward magnetic field (B_Z), and interplanetary coronal mass ejections speed (V) is found empirically by Gopalswamy, which is given as $Dst = -0.01VB_Z - 32nT$. For $B_Z = 55nT$ and $V = 1000\frac{km}{sec.}$, we obtain $Dst = -582nT$ which is nearly the recorded value on March $13 - 14$, 1989 geomagnetic storm. Therefore, both southward IMF (B_Z) and speed of ICME are the most important parameters related to the sources of magnetized plasma from the solar corona, which in turn cause severe geomagnetic storm.

   The probability of major solar storm follows the 11-year sunspot cycle. This is the time when sunspot activity increases from its minimum to maximum and returns to its minimum. The amount of CMEs ejected from the solar corona is also expected to be follow this season. This is also the time when CME directed towards the earth and cause geomagnetic storms as well as geomagnetically induced currents. The effect of CME increases during solar maximum because of sunspots activity. That is, the occurance of CME has a roughly linear relationship with the number of sunspots. So we expect the earthward CME cause geomagnetic storms during the maximum solar cycles. To observe sunspot activity, we used data from Solar Influences Data analysis Center (SIDC), Royal Observatory of Belgium and we plotted the yearly sunspot number from 1950 to 2009 as shown in the Fig.4.1. The graph

covered from about solar cycle 19 to cycle 23: solar cycle 19 (1954–1964), cycle 20 (1964–1976), cycle 21 (1976–1986), cycle 22 (1986–1996), and cycle 23 (1996–2008). There are about 5.4 complete sunspot cycles. So, in the interval of 1950 to 2009 the average solar cycle is about 10.9 years as shown in the Fig.4.1. Thus, our graph verify complete solar cycle from the minimum to maximum, and back to the minimum takes approximately 11-years. The major sunspot maximum was occured in 1957 during cycle 19, in 1969 during cycle 20, in 1980 during cycle 21, in 1989 during cycle 22, and in 2002 during cycle 23 as shown in the Fig.4.1. However, major geomagnetic storm was occured in the years 1960, 1972, 1982, 1989, and 2003 as discussed in [61]. Among these the 1989 and 2003 geomagnetic storms were severe on earth as recorded in space age era. These geomagnetic storms were occured during the maximum phase and declining phase of solar activity as we marked in the Fig.4.1. During the sunspot maximum geomagnetic storms are mainly driven by coronal mass ejections (CMEs) as occured in 1989.

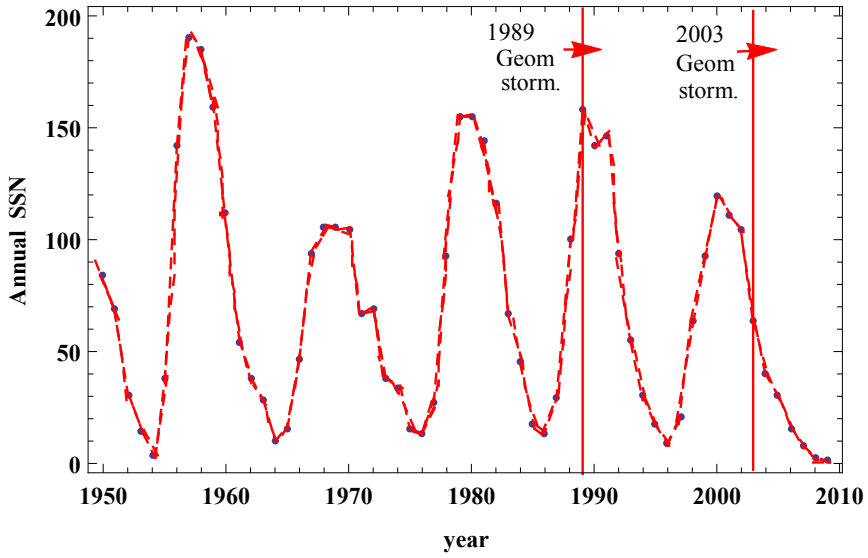

Figure 4.1: The yearly-averaged number of sunspots visible on the sun from 1950–2009. The two vertical lines are to show the correlation of SSN with the severe geomagnetic storms.

2. Dst-index and geomagnetic storm

We use Dst-index to descuss the CMEs responsible for intense geomagnetic storms. To describe this we used hourly equitorial Dst data from the World Data Center (WDC) in Kyoto, Japan. From this data we selected March 12–14 dst1989, October 29–31 dst2003 and November 19–21 dst2003 because of

their severe geomagnetic storms on earth during the solar cycle 22 and cycle 23.

Using March 12–14 dst1989 data, we plotted the 1989 extreme geomagnetic storm. We used hourly dst data, then the time interval plot goes from 0 to 72 hours for three days. The first 24 hours ($12^{th} March$) indicates that the storm quiet phase, the second 26 hours ($13^{th} March$) indicates that storm main phase with SSC at initial for 2 hours, and the last 22 hours ($14^{th} March$) is considered as storm recovery phase. The minimum peak Dst-index value is about $-589nT$ as shown in the Fig.4.2. This is in the range of extreme geomagnetic storm and happened at about 1 hour on March 14, 1989 which is at the end of the storm main phase.

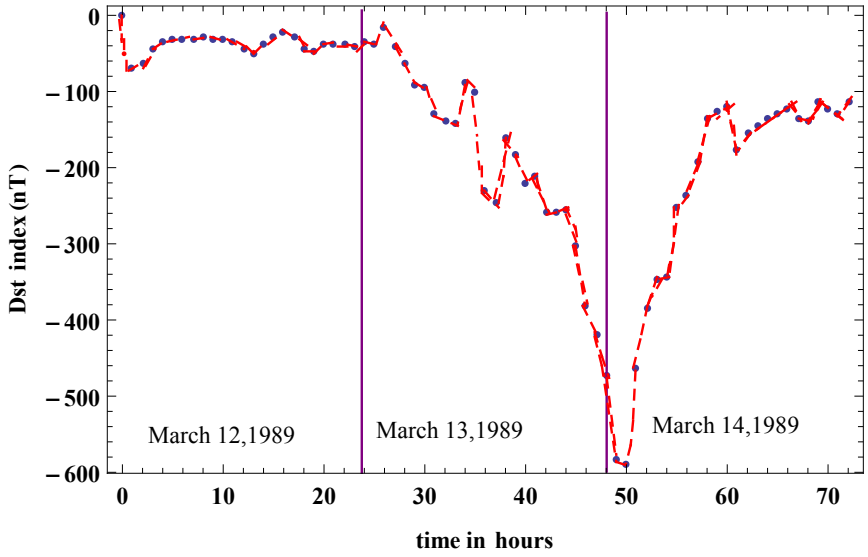

Figure 4.2: Hourly Dst-index graph for the March 13–14, 1989 extreme geomagnetic storm, plotted for three days

We also plotted using March 1–31 dst1989 data in the range of the minimum Dst-index value at a particular time of 2 hours each days. It is also followed by nearly storm quiet phase (March 1–12), SSC (March 12–13), storm main phase (March 13–14), and storm recovery phase (March 15–31). We also observed that the 1989 extreme geomagnetic storm of Dst-index value $-589nT$ is correlated with the maximum sunspot activity as shown in the Figs.4.1 and 4.3.

Another geomagnetic storm which included in our discusion is the Oct–Nov 2003 storm. Using October 29–31 dst2003 from the World Data Center (WDC) Kyoto, we plotted its hourly Dst-index graph as shown in the Fig.4.4. The

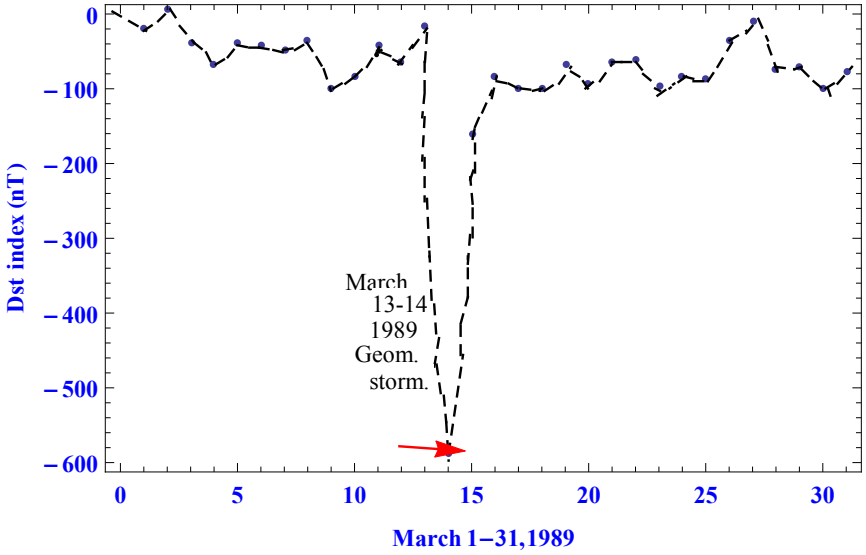

Figure 4.3: Daily-disturbance storm time (Dst) index graph on March 1989 at a particular time of 2 hours.

graph shows different storm progresses: storm initial phase (SSC) is for the first 7 hours and the storm main phase is for the second 18 hours with peaked at a Dst-index value of $-353nT$. Although the storm is gradually return for the third 17 hours, its Dst-index value is still about hundreds of negative nT. That is, the storm didn't return to its steady state (recovery phase) at all in this range. The storm is back to the main phase for the fourth 6 hours and reaches the minimum Dst-index value of about $-400nT$. This is the most likely in the range of superintense geomagnetic storm and it is correlated with the SSN as shown in the Fig.4.1. Finally the storm is gradually return back to its recovery phase for the last 22 hours as shown in the Fig.4.4.

Similarly, we plotted hourly Dst-index on November 19–21, 2003 geomagnetic storm peaked at a Dst-index value of $-422nT$ as shown in the Fig.4.5. Our graph is agreement with all of the storm phases. During Nov 19, 2003 the storm was in a steady (quiet phase) which is most likely as CME is not interact with the earth's magnetic field. At the end of the quiet phase there was storm initial phase (SSC) which is most likely as the leading edge of CME arrive at earth's magnetosphere. During Nov 20, 2003 there was storm main phase which is most likely as the CME driving by solar wind compress or, even penetrate the magnetosphere due to the magnetic reconnection and increases ring current density in the radiation belts. Eventhough the storm is peaked at a Dst-index of $-422nT$, there was no fault recorded on infrastructures

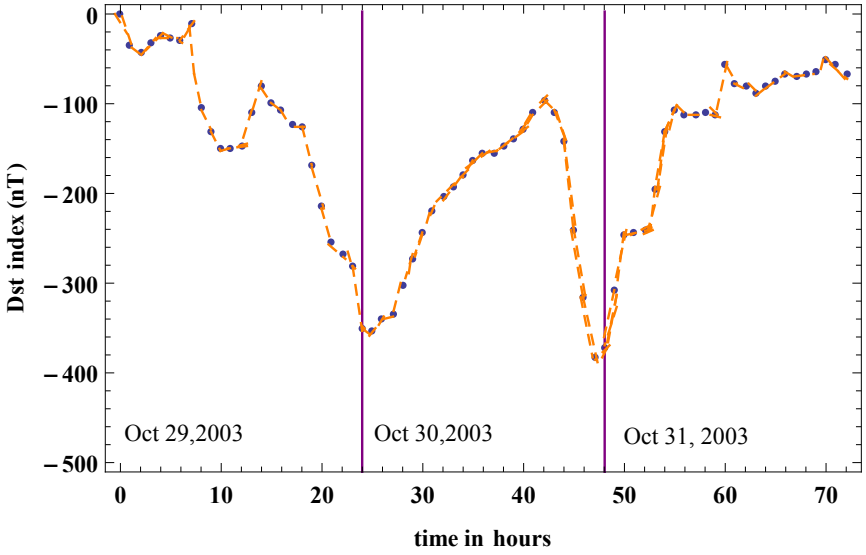

Figure 4.4: Three consecutive days of hourly Dst-index graph for the October 29–31, 2003 geomagnetic storm

during this time. During Nov 21, 2003 there was storm recovery phase which indicates the storm returns to its quiet phase as the ring current density decreases as shown in the Fig.4.5.

Moreover, CMEs are responsible for the geomagnetic storms of 1989 (the hydro-Quebec storm), and 2003 storm (the Halloween geomagnetic storm) are well correlated [51, 53]. During such event the earth is magnetically connected with maximum sunspot activity. We marked vertical lines to relate sunspot activity with these major geomagnetic storms as shown in the Fig.4.1. The hydro-Quebec event was on the March 13–14, 1989 geomagnetic storm that was responsible for the Quebec power blackout in Canada and North America durng the end of storm main phase of the negative peak value of Dst-index $\sim -589nT$ (i.e, during the maximum phase of sunspot activity) as shown in the Figs.4.1 and 4.2. On the October–November 2003, storm is also called Halloween storm which was responsible for power blackout in Sweden on October 30, 2003 during the storm recovery phase (i.e, during the declining phase of sunspot activity), and also was severe damage to power grids in South Africa on October 29, 2003 during storm main phases. Therefore, geomagnetic storms would cause power blackout during the storm main phases as well as during storm recovery phase whose Dst-index value is approaching about hundreds of negative nT as shown in the Figs.4.4 and 4.5. That means, CMEs wich in turn give GICs are the prime cause of power blackout in 1989

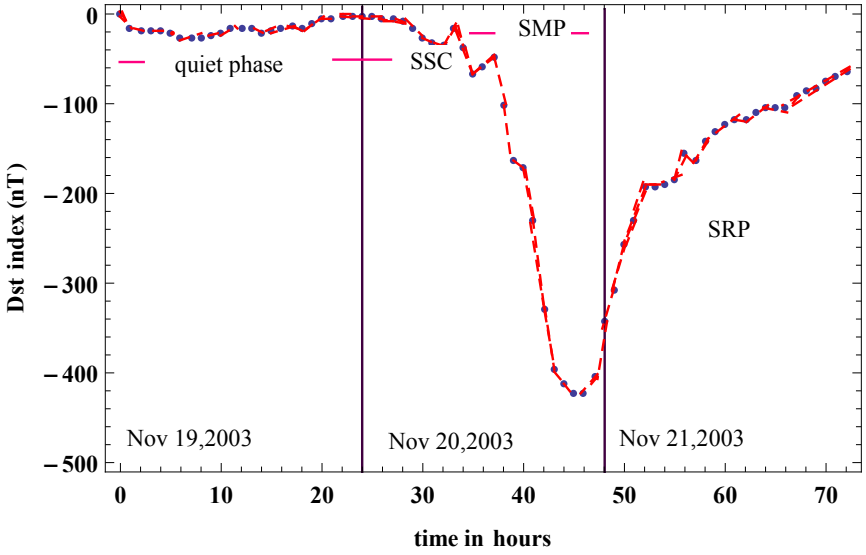

Figure 4.5: Three consecutive days of hourly Dst-index graph for the Nov.20–21, 2003 geomagnetic storm. It is followed by quiet phase, sudden storm commencement (SSC), storm main phase (SMP), and storm recovery phase (SRP)

and 2003 due to their severe geomagnetic storms. Both CMEs and maximum sunspot activity are correlated, which in turn gives geomagnetic storm as well as the negative peak value of Dst-index as seen in the Figs.4.1–4.5.

3. Earth's surface impedance and its penetration depth

   In the above sections we discussed coronal mass ejections as the prime cause for geomagnetic storms in relation to solar cycle and disturbance storm time (Dst) index. In this section we will discuss geomagnetically induced current (GIC) density during the main geomagnetic storms according to Faraday's law of induction and Ohm's law. In addition, the nature of earth's surface impedance and its penetration depth related to geographical conditions such as igneous rock location with high resistivity and low conductivity will be observed in the Figs.4.6 and 4.7. So, using Eqn.(3.22) we plotted earth's surface impedance as a function of angular fruquency by assuming local ground conductivity is uniform. The graph shows that an overall exponential increase in the earth's surface impedance with angular frequency of GIC. As the angular frequency increases from about 0.0006–0.06 $\frac{rad}{sec}$ then earth's surface impedance increases exponentially from about 0 to 7000 ohms as seen in the Fig. 4.6. We suggest that, the ground impedance arise due to geomagnetically induced currents to oppose the field variations that is causing it. Again, using Eqn.(3.12)

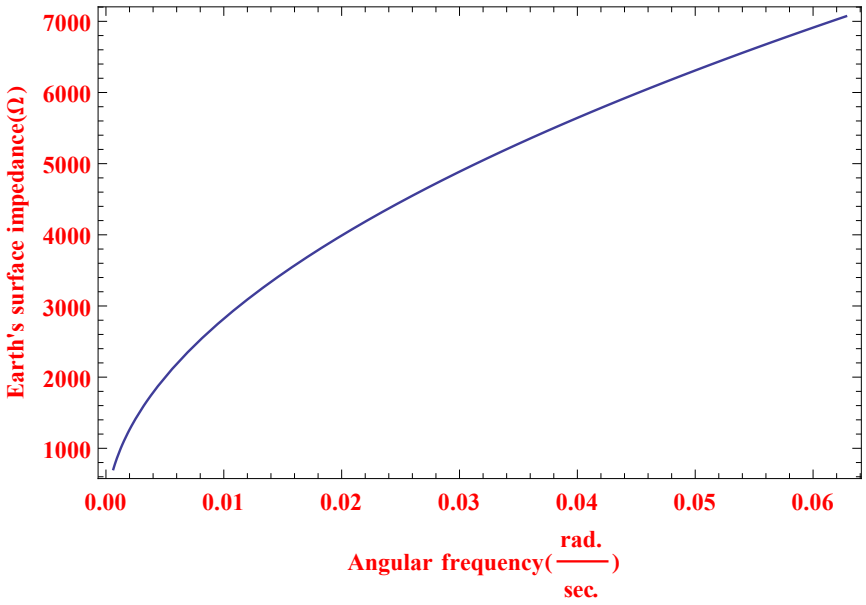

Figure 4.6: Earth's surface impedance as function of angular frequency. The parameters used are $\omega = 0.0006 - 0.06\frac{rad}{sec}$, $\sigma = 0.001\frac{S}{m}$ and $\mu_\circ = 4\pi \times 10^{-7}\frac{H}{m}$

we plotted the earth's penetration depth as a function of field's frequency by considering local ground conductivity is uniform. The graph shows penetration depth is an exponentially decreasing rapidily from about 600000 m to zero as its frequency range increases from about 0.0001–0.01Hz as seen in the Fig.4.7. That is, the amplitude of the electric and magnetic fields as well as current density are exponentially decay as frequency increases. On the other hand, the ground resistivity can varies from one location to another. So that the effect of GIC on any man-made electrically connected to the ground is not uniform. That is, the impact of GIC on power transmission depends on the local ground resistivity. The higher the resistivity; the less depth penetration into the earth, and could be impacts on power transmission that are electrically connected to the earth.

4. Diffusion current density

   Using the imaginary part of Eqn.(3.21), we plotted the diffusion current density as a function of inward distance to the earth's center for different time instant of angular distance measured in radians. We used local ground resistivity of about $\sigma = 0.001\frac{s}{m}$ based on geological survey of Canada and $B_{space} = 500nT$ where severe geomagnetic storm such as March 13–14, 1989 was occured. In addition, usual frequency range of geomagnetically induced current (GIC) is 0.0001–0.01Hz according to [70, 71, 72]. From this frequency range in

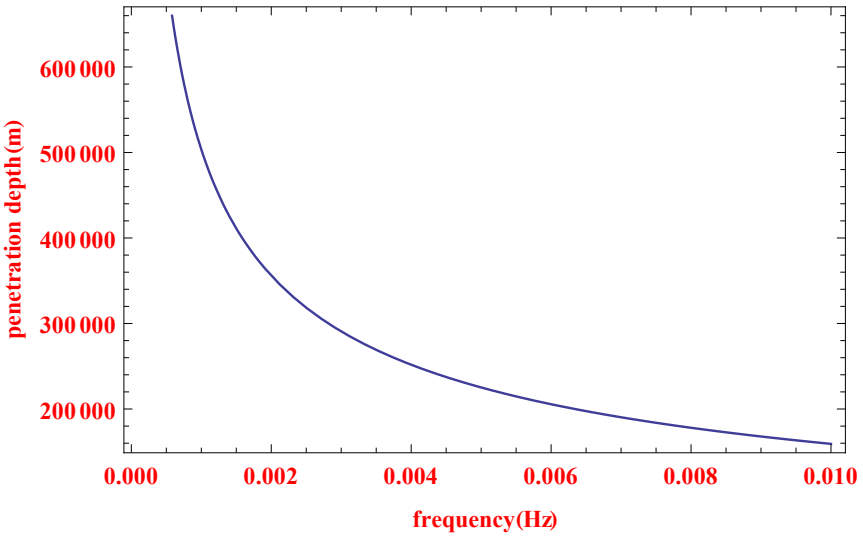

Figure 4.7: The penetration depth as function of frequency. The parameters used are $\nu = 0.0001 - 0.01Hz$, $\sigma = 0.001\frac{s}{m}$ and $\mu_\circ = 4\pi \times 10^{-7}\frac{H}{m}$

Hz we selected 0.002, 0.004, 0.006, 0.008 and 0.010. Their correspondence time period in seconds are 500, 250, 167, 125, and 100. In view of these, their correspondence angular frequencies in $\frac{rad.}{sec}$ are 0.01, 0.03, 0.04, 0.05 and 0.060. These different angular frequencies at different time instant give different angular distances of diffusion current density during one cycle which displayed as a, b, c, d, and e. Graphs a, b, c and e are just in phase in view of graph d as seen in the Fig.4.8. Moreover, the graph is just a sample of diffusion current density result for different angular frequencies at different time instant of angular distance that are travelling in opposite directions. The positive and negative current densities are both about $2 \times 10^{-6}\frac{A}{m^2}$ at the ground level. However, they all show a decrease in the intensity of the current density values towards the earth center as seen in the Fig.4.8.

The graph decreases exponentially towards the earth's center due to $e^{\frac{-z}{\delta}}$. At about 1.539×10^5m of (the penetration depth) distance, the amplitude of the current density decreases to about one-third (0.37) of the original value as seen in the Fig.4.8. The positive and negative value of current density in the graph indicates for east-west current density which is sensitive to geomagnetic storm due to the variation of north-south component of earth's magnetic field. When magnetic reconnection takes place at the earth's dayside, diffusion current is mostly towards east direction. When magnetic reconnection takes place at the earth's nightside diffusion current is mostly towards the west direction.

In the magnetic diffusion process, diffusion current flows in a direction opposite to the penetration of the magnetic field as discussed in [53]. Which means geomanetic storm is the prime cause for diffusion current. The magnetic diffusion and diffusion current attenuate exponentially to zero because of $e^{\frac{-z}{\delta}}$ where δ is penetration depth given by $\delta = \sqrt{\frac{2}{\sigma\omega\mu_\circ}}$. That is, the solar wind transfers plasma, momentum and energy into the earth's magnetosphere. It distorts the dipole of magnetic fields of the earth, compressing the dayside (sunward side) and drawing the nightside (anti-sunward side) out into a magnetotail. So on the dayside the induced currents and fields, usually points into eastward direction. On the nightside of magnetotail reconnection, the global pattern of convection in magnetosphere is from nightside to dayside (opposite to the direction of solar plasma). This gives on the nightside there is also induced currents and fields directed westward. When the energised electron content in radiation belt decreases; amplitudes of the field decay exponentially towards earth center on both dayside and nightside as seen in the Fig.4.8. From the above discussion we suggest that, east-west current density can be induced in the solid body of the earth during severe geomagnetic storm. This ground current density can cause problem in any man-made infrastructures that are electrically connected to earth.

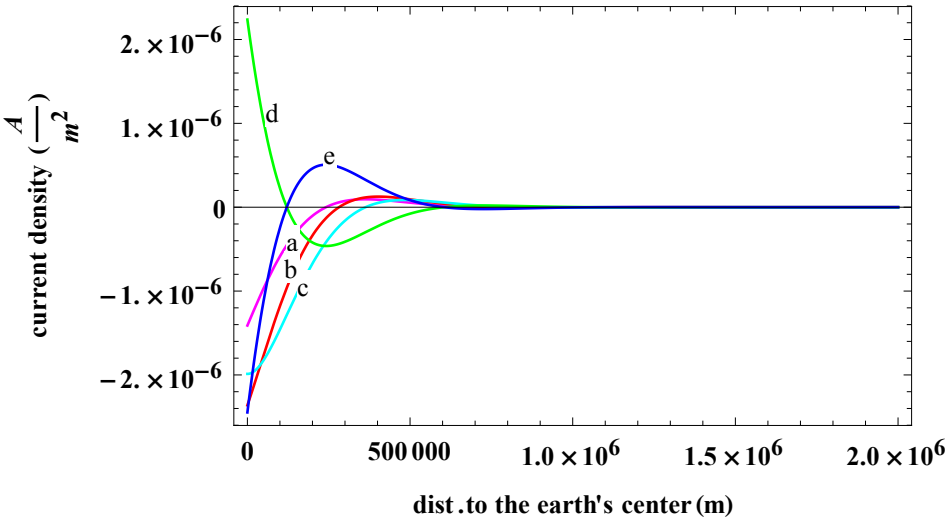

Figure 4.8: Graph of diffusion current density as function of inward distance(z) to the earth's center for different time instant of angular distance(ωt): a, b, c, d and e indicates for $\frac{\pi}{4}$, $\frac{\pi}{3}$, $\frac{\pi}{2}$, π and 2π radians; frequency(ν): 0.002, 0.004, 0.006, 0.008 and 0.010 Hz; period(T): 500, 250, 167, 125 and 100 seconds; angular frequency(ω): 0.01, 0.03, 0.04, 0.05 and 0.06 $\frac{rad}{sec}$; time instant(t): $\frac{T}{8}$, $\frac{T}{6}$, $\frac{T}{4}$, $\frac{T}{2}$ and T respectivily.

CHAPTER 5

Conclusion

Ejections of magnetized plasma of matter on the solar corona called coronal mass ejections (CMEs) can lead to southward interplanetary magnetic fields in the resulting geomagnetic storms as well as geomagnetically induced currents (GICs). The probability of CME hitting the earth and its causing geomagnetic storm depends on its angular breadth, speed, orientation and strength. Moreover, their causing geomagnetic storms are more common during the sunspot activity phase. Based on present concept, major geomagnetic storm occurs if there is a strong southward component of magnetic field and high-speed of interplanetary coronal mass ejection. Severity of geomagnetic storms are measured by a very common index called disturbance storm time (Dst) index. It indicates the average change of the earth's horizontal magnetic field in units of nT, located at the four low-latitude magnetic observatories. Severe geomagnetic storms are expressed as high negative Dst-index. On the other side, the sunspot number (SSN) is the commonly used index to measure solar activity phase. They are regions of intense magnetic field and the prime cause for coronal mass ejections (CMEs).

In this thesis we reviewed the relation of sunspot activity and disturbance storm time (Dst) index with strong coronal mass ejections (CMEs) as the prime cause for severe geomagnetic storms that in turn produce geomagnetically induced currents (GICs). So that we discussed the effects of coronal mass ejections on the geospace (i.e, on the modern techonolgies and space weathers) interms of their potential to generate major geomagnetic storms that lead to geomagnetically induced currents. We also presented a simple derivation of the magnetic diffusion and ground current density during massive earthward CMEs. This analytical approach helps us for examining the effects of geomagnetic storms on the modern technologies. In general, we reviewed some basic ideas of the effects resulting from solar corona-earth connections, with emphasis on major geomagnetic storms during strong coronal mass ejections.

We considered yearly sunspot number during solar cycle 22 and solar cycle 23. From these we selected 1989 geomagnetic storm durng solar cycle 22 and 2003 geomagnetic storm during solar cycle 23 because they were severe as well as known for their power blackout as recorded in space age era. We also considered hourly Dst-index on March 12–14, 1989 and on October–November 2003, and related them with the sunspot activity phase. We analysed that the 1989 extreme geomagnetic storm of minimum peak Dst-index value of $\sim -589nT$ was correlated with the maximum peak of sunspot number. It is believed that sunspot maximum phase means the period of intense magnetic field and major ejected magnetized plasma from solar corona. Hence, we suggested that during the sunspot maximum, severe geomagnetic storms are mainly driven by coronal mass ejections (CMEs) as occured in 1989. However, during 2003 geomagnetic storm of minimum peak Dst-index value of $\sim -400nT$, it is correlated with the declining phase of sunspot number. During this it is believed that geomagnetic storms are mainly driven by corotating interaction region storms. In genaral, severe geomagnetic storms that have an effect on modern technologies can be occured during declining sunspot number (storm recovery phase), in addition to during the maximum sunspot number (storm main phase). Thus, we suggested that CMEs and sunspot activities are correlated in driving major geomagnetic storms.

Furthermore, we computed north-south magnetic diffusion using plane wave method that lead to east-west electric field and geomagnetically induced current density as well. We analysed a sample of diffusion current density resulted for different angular frequencies at different time instant of angular distances during one cycle. We suggested that the positive and negative ground current densities (that are travelling in opposite directions) are both about $2 \times 10^{-6} \frac{A}{m^2}$ on the east-west side. Though they all show an exponentially decrease in the intensity of the current density values towards the earth center. We also suggested that such east-west current density during extreme CMEs can cause problem in power transmissions that are connected to area of high ground resistivity.

As a suggestion for future work, I try to explore more the effects resulting from sun-earth connections, using relevant observations, computational tools and data with emphases on coronal mass ejections.

Bibliography

[1] Janvier, Miho and Winslow, Reka M and Good, Simon and Bonhomme, Elise and Démoulin, Pascal and Dasso, Sergio and Möstl, Christian and Lugaz, Noé and Amerstorfer, Tanja and Soubrié, Elie and others. Generic Magnetic Field Intensity Profiles of Interplanetary Coronal Mass Ejections at Mercury, Venus, and Earth From Superposed Epoch Analyses. Journal of Geophysical Research: Space Physics, Wiley Online Library, 2019.

[2] Morosan, DE and Kilpua, EKJ and Carley, EP and Monstein, C. Variable emission mechanism of a Type IV radio burst. Astronomy & Astrophysics, EDP Sciences, 2019.

[3] David F. Webb, Timothy A. Howard. Coronal Mass Ejections: Observations. Solar Phys., 9, 2012.

[4] Gopalswamy, Nat. Coronal Mass Ejections: a Summary of Recent Results. Slovak Central Observatory, page 108–130, 2010.

[5] Gopalswamy, S and Akiyama, S and Yashiro, and Mäkelä, P. Coronal Mass Ejections from Sunspot and Non-Sunspot Regions. Springer, page 289–307, 2010.

[6] Gopalswamy, Nat. Coronal Mass Ejections: a Summary of Recent Results. Slovak Central Observatory, page 108–130, 2010.

[7] H.S. Hudson 1, J.L. Bougeret and J. Burkepile. Coronal mass ejections: Overview of observations. Space science reviews, 00: 1–20, 2006.

[8] Saumitra Mukherjee. Cosmic Influence on the Sun-Earth Environment. Geology and Remote Sensing, 2008.

[9] Mike Hapgood. Space Weather. IOP Publishing, Bristol, UK, 2019.

[10] Labrosse, N and Heinzel, P and Vial, J-C and Kucera, T and parenti, S and Gunßr, S and Schmieder, B and Kilper, G. physics of solar prominences. Space Science Reviews, pages 243–332, 2010.

[11] https://openstax.org/details/books/astronomy. Rice University, 2018.

[12] Malcolm S. Longair. High energy Astrophysics. Cambridge University Press, New York, 2011.

[13] Arun Babu K.P. Coronal Mass Ejections from the Sun-Propagation and Near Earth Effects. Astro-phy thesis, 2014.

[14] Bradley W. Carroll Dale A. Ostlie. An Introduction to Modern Astrophysic. Pearson Education Limited, 2014.

[15] Jeffrey Bennett. The cosmic perspective. Pearson Addison-Wesley, 2010.

[16] Erdelyi, R.; Ballai, I. Heating of the solar and stellar coronae: a review. Astron. Nachr, 2007.

[17] Alfven, H. Magneto-hydrodynamic waves, and the heating of the solar corona. Monthly Notices of the Royal Astronomical Society, 1947.

[18] Nat Gopalswamy. Coronal mass ejections as a new indicator of the active sun. International Astronomical Union, 2018.

[19] Erika Bohm-Vitense. Introduction to stellar Astrophysics. Cambridge University press, 2003.

[20] John Wiley and Sons Ltd. An introduction to stellar astrophysics. Francis LeBlanc, 2010.

[21] Chrbonneau, Paul. Dynamo models of the solar cycle. Living Reviews in solar physics, Springer 2010.

[22] Gopalswamy, N and Yashiro, S. The soho/lasco cme catalog. Springer, pages 295–313, 2009.

[23] Yurchyshn, V and Yashiro, S and Abramenko, V and Gopalswamy, N. Statistical distributions of speeds of coronal mass ejections. The Astrophysical journal, IOP Publishing, pages 599, 2005.

[24] Vourlidas, Angelos and Howard, Russ A and Esfandiari, Ed and Patsourakos, Spiros and Yashiro, Seiji. Comprehensive analysis of coronal mass ejection and energy properties over a full cycle. The Astrophysical journal, IOP Publishing, pages 1522, 2010.

[25] Veronig. Genesis and impulsive evolution of the 2017 September 10 coronal mass ejection. The Astrophysical journal, IOP Publishing, pages 107, 2018.

[26] E. W. Cliver and L. Svalgaard. The 1859 solar-terrestrial disturbance and the current limits of extreme space weather activity. Sol.Phys., pages 407–422, 2004.

[27] Lindemann, F. Note on the theory of magnetic storms. Philosophical magazine series, page 21, 1919.

[28] Forbush, S.E. Three unusual cosmic-ray increases possibly due to charged particles from the sun. Physical review, pages 771–772, 1919.

[29] Kahler, S.W. Solar sources of heliospheric energetic electron events-shocks or flares? Space science reviews, pages 359–390, 2007

[30] Sheeley Jr, NR and Michels, DJ. Initial observations with the Solwind coronagraph. The astrophysical journal, volume 237, pages L99–L1O1, 1980.

[31] Babu, Arun. Coronal Mass Ejections from the Sun-Propagation and Near Earth Effects. arXiv preprint arXiv: 1407.4258, 2014.

[32] Brueckner, GE and Howard, RA and Koomen, MJ and Korendyke, CM and Michels, DJ and Moses, JD and Socker, DG and Dere, KP and Lamy, PL and Llebaria, A and others. The large angle spectroscopic coronagraph (LASCO). The SOHO Mission, pages 357–402, 1995.

[33] Hirayama, Tadashi and Nakagomi, Yoshiteru. Observations of prominences in He II with a new 25 CM coronagraph. Publications of the Astronomical Society of Japan, volume 26, pages 53, 1974.

[34] Eddy, JOHN A. The Sun, the Earth, and near-Earth space. US Government printing office, Washington, DC, 2009.

[35] Yashiro, N. A catalog of white light coronal mass ejections observed by the SOHO spacecraft. J. Geophys., 2004.

[36] Gopalswamy, N. A Global Picture of CMEs in the inner heliosphere. Astrophysics and Space Science Library, vol.317, pages 201–251, 2004

[37] Illing, R.M.E.and Hundhausen, A.J. Observation of a coronal transient from 1.2 to 6 solar radii. Journal of Geophysical Research, pages 275–282, 1985.

[38] Howard, R.A., Michels, D.J., Sheeley Jr, N.R. and Koomen, M.J. The observation of a coronal transient directed at Earth. Astrophys. J., pages L101–L104, 1982.

[39] Howard, TA and DeForest, CE. The Thomson surface. I. Reality and myth. The Astrophysical Journal, number 2, pages 130, 2012.

[40] Su, Yingna and Surges, Vincent and Van Ballegooijen, Adriaan and DeLuca, Edward and Golub, Leon. Observations and magnetic field modeling of the flare/coronal mass ejection event on 2010 April 8. The Astrophysical Journal, volume 734, pages 53, 2011.

[41] Schrijver, CarolusJ and Elmore, Christopher and Kliem, Bernhard and Török, Tibor and others. Observations and modeling of the early acceleration phase of erupting filaments involved in coronal mass ejections. The Astrophysical Journal, IOP Publishing, volume 674, pages 589, 2008.

[42] Priest, ER and Schrijver, CJ. Physics of the Solar Corona and Transition Region. Springer, pages 1–24, 2000.

[43] Lin, J and Forbes, TG. Journal of Geophysical Research: Space Physics. Journal of Geophysical, numberA2, pages 2375–2392, 2000.

[44] Antiochos, SK and DeVore, CR and Klimchuk, JA. A model for solar coronal mass ejections. The Astrophysical Journal, volume 510, pages 485, 1999.

[45] Lynch, BJ and Antiochos, SK and DeVore, CR and Luhmann, G and Zurbuchen, TH. Topological evolution of a fast magnetic breakout CME in three dimensions. The Astrophysical Journal, volume 683, pages 1192, 2008.

[46] Marusek, James A. Solar storm threat analysis. J. Marusek, 2007.

[47] Dumbović, Mateja. Analysis and forecasting of coronal mass ejection space weather effects. Prirodoslovno-matematički fakultet, Sveučilišteu Zagrebu, 2015.

[48] Wright, Andrew N and Rickard, Graham J. A numerical study of resonant absorption in a magnetohydrodynamic cavity driven by a broadband spectrum. The Astrophysical Journal, volume 444, pages 458–470, 1995.

[49] Bothmer, Volker and Daglis, Ioannis A. Space weather: physics and effects. Springer Science & Business Media, 2007.

[50] Haynes, Peter and Shuckburgh, Emily. Effective diffusivity as a diagnostic of atmospheric transport: 1.Stratosphere. Journal of Geophysical Research: Atmospheres, volume 105, pages 22777–22794, 2000.

[51] Oliveira, Denny M and Ngwira, Chigomezyo M. Geomagnetically induced currents: Principles. Brazilian Journal of Physics, volume 47, number 5, pages 552–560, 2017.

[52] Mukherjee, Saumitra. Cosmic influence on the sun-earth environment. Sensors, volume 8, number 12, pages 7736–7752, 2008

[53] Sidhu, Rajbir Kaur. Impacts of Geomagnetic Storms on Trans-Canadian Grids. McGill University Library, 2010.

[54] Michalek, G and Gopalswamy, N and Lara, A and Yashiro, S. Properties and geoeffectiveness of halo coronal mass ejections. Space Weather, volume 4, number 10, pages 1–17, 2006.

[55] Webb, DF and Cliver, EW and Crooker, NU and St. Cyr, OC and Thompson, BJ. Relationship of halo coronal mass ejections, magnetic clouds, and magnetic storms. Journal of Geophysical Research: Space Physics, volume 105, number A4, pages 7491–7508, 2000.

[56] Schrijver, Carolus J. Socio-economic hazards and impacts of space weather: The important range between mild and extreme. Space Weather, volume 13, number 9, pages 524–528, 2015.

[57] Rubin, Harvey and others. Future Global Shocks: Pandemics. OECD, 2011.

[58] Chavalier, G. The Earth's Electrical Surface Potential. A Summary of Present Understanding. California Institute for Human Science, Encinitas, 2007.

[59] Thorberg, Rasmus. Risk analysis of geomagnetically induced currents in power systems. Division of Industrial Electrical Engineering and Automation Faculty of Engineering, LTH, Lund University, 2012.

[60] Watermann, J. Space Weather Effects Observed on the Ground-Geomagnetic Effects. First European Space Weather Week (ESWW), ESA-Estec, Noordwijk, 2004.

[61] Roodman, D. The risk of geomagnetic storms to the grid: A preliminary review. , 2015.

[62] Campbell, Wallace H. An interpretation of induced electric currents in long pipelines caused by natural geomagnetic sources of the upper atmosphere. Surveys in Geophysic, volume 8, number 3, pages 239–259, 1986.

[63] Liu, Chunming and Ganebo, Yared Senbato and Wang, Hongmei and Li, Xinjie. Geomagnetically Induced Currents in Ethiopia Power Grid: Calculation and Analysis. IEEE Access, volume 6, pages 64649–64658, 2018

[64] Woodson, Herbert H and Melcher, James R. Electromechanical Dynamics: Fields, forces, and motion. Wiley, 1968.

[65] Lomon, Earle L. Classical Electrodynamics. American Association for the Advancement of Science, 1962.

[66] Løseth, Lars O and Pedersen, Hans M and Ursin, Bjørn and Amundsen, Lasse and Ellingsrud, Svein. Low-frequency electromagnetic fields in applied geophysics: Waves or diffusion? Geophysics, volume 71, number 4, pages w29–w40, 2006.

[67] Pirjola, Risto. Geomagnetically induced currents as ground effects of space weather. Space Science, pages 27–44, 2012.

[68] De Villiers, JS and Pirjola, RJ and Cilliers, PJ. Estimating ionospheric currents by inversion from ground-based geomagnetic data and calculating geoelectric fields for studies of geomagnetically induced currents. Earth, Planets and Space, volume 68, number 1, pages 154, 2016.

[69] Alekseev, Dmitry and Kuvshinov, Alexey and Palshin, Nikolay. Compilation of 3D global conductivity model of the Earth for space weather applications. Earth, Planets and Space, volume 67, number 1, pages 108, 2015.

[70] Boteler, DH and Pirjola, RJ. Modeling geomagnetically induced currents. Space Weather, volume 15, number 1, pages 258–276, 2017.

[71] Liu, Chun-Ming and Liu, Lian-Guang and Pirjola, Risto and Wang, Ze-Zhong. Calculation of geomagnetically induced currents in mid-to low-latitude power grids based on the plane wave method: A preliminary case study. Space Weather, volume 7, number 4, 2009.

[72] Liu, Chunming and Li, Yunlong and Pirjola, Risto. Observations and modeling of GIC in the Chinese large-scale high-voltage power networks. Journal of Space Weather and Space Climate, volume 4, pages A03, 2014.

[73] Van de Hulst, HC and others. The electron density of the solar corona. Bulletin of the Astronomical Institutes of the Netherlands, pages 135, 1950.

[74] Vourlidas, A and Buzasi, D and Howard, RA and Esfandiari, E. Mass and energy properties of LASCO CMEs. Solar variability: from core to outer frontiers, volume 506, pages 91–94, 2002.

[75] Chen, James. Effects of toroidal forces in current loops embedded in a background plasma. The Astrophysical Journal, volume 338, pages 453–470, 1989.

[76] Munro, RH and Gosling, JT and Hildner, E and Macqueen, RM and Ploland, AI and Ross, CL. The association of coronal mass ejection transients with other forms of solar activity. Springer, Solar physics, volume 61, number 1, pages 201–215, 1979.

[77] Hudson, Hugh S and Webb, David F. Soft X-ray signatures of coronal ejections. Geophysical Monograph American Geophysical Union, volume 99, pages 27–38, 1997.

DECLARATION

ADDIS ABABA UNIVERSITY
COLLEGE OF NATURAL AND COMPUTATIONAL SCIENCES
DEPARTMENT OF PHYSICS

MSc Thesis

Coronal Mass Ejections and Problem they Cause on Earth

Name of Candidate: Debela Alemayehu Gashe

I the under signed declare that the thesis is my original work and no part of it can be claimed as an intellectual property of anybody else except me and my advisors.

Signature: _____